Article

Economic Feasibility of Power/Heat Cogeneration by Biogas–Solid Oxide Fuel Cell (SOFC) Integrated Systems

Costas Athanasiou [1] , Christos Drosakis [2] , Gaylord Kabongo Booto [3,4] and Costas Elmasides [1,*]

[1] Department of Environmental Engineering, Democritus University of Thrace, 67100 Xanthi, Greece
[2] Department of Mechanical Engineering, University of Western Macedonia, 50100 Kila Kozanis, Greece
[3] Environmental Impacts & Sustainability, NILU—Norwegian Institute for Air Research, Instituttveien 18, 2007 Kjeller, Norway
[4] Norwegian Institute for Sustainability Research (NORSUS), Stadion 4, N-1671 Kråkerøy, Norway
[*] Correspondence: kelmasid@env.duth.gr; Tel.: +30-25410-79876

Abstract: Based upon the thermodynamic simulation of a biogas-SOFC integrated process and the costing of its elements, the present work examines the economic feasibility of biogas-SOFCs for combined heat and power (CHP) generation, by the comparison of their economic performance against the conventional biogas-CHP with internal combustion engines (ICEs), under the same assumptions. As well as the issues of process scale and an SOFC's cost, examined in the literature, the study brings up the determinative effects of: (i) the employed SOFC size, with respect to its operational point, as well as (ii) the feasibility criterion, on the feasibility assessment. Two plant capacities were examined ($250 \ m^3 \cdot h^{-1}$ and $750 \ m^3 \cdot h^{-1}$ biogas production), and their feasibilities were assessed by the Internal Rate of Return (IRR), the Net Present Value (NPV) and the Pay Back Time (PBT) criteria. For SOFC costs at 1100 and 2000 $EUR \cdot kW_{el}^{-1}$, foreseen in 2035 and 2030, respectively, SOFCs were found to increase investment (by 2.5–4.5 times, depending upon a plant's capacity and the SOFC's size) and power generation (by 13–57%, depending upon the SOFC's size), the latter increasing revenues. SOFC-CHP exhibits considerably lower IRRs (5.3–13.4% for the small and 16.8–25.3% for the larger plant), compared to ICE-CHP (34.4%). Nonetheless, according to NPV that does not evaluate profitability as a return on investment, small scale biogas-SOFCs (NPV_{max}: EUR 3.07 M) can compete with biogas-ICE (NPV: EUR 3.42 M), for SOFCs sized to operate at 70% of the maximum power density (MPD) and with a SOFC cost of 1100 $EUR \cdot kW_{el}^{-1}$, whereas for larger plants, SOFC-CHP can lead to considerably higher NPVs (EUR 12.5–21.0 M) compared to biogas-ICE (EUR 9.3 M). Nonetheless, PBTs are higher for SOFC-CHP (7.7–11.1 yr and 4.2–5.7 yr for the small and the large plant, respectively, compared to 2.3 yr and 3.1 yr for biogas-ICE) because the criterion suppresses the effect of SOFC-CHP-increased revenues to a time period shorter than the plant's lifetime. Finally, the economics of SOFC-CHP are optimized for SOFCs sized to operate at 70–82.5% of their MPD, depending upon the SOFC cost and the feasibility criterion. Overall, the choice of the feasibility criterion and the size of the employed SOFC can drastically affect the economic evaluation of SOFC-CHP, whereas the feasibility criterion also determines the economically optimum size of the employed SOFC.

Keywords: biogas; SOFC; simulation; economic feasibility

1. Introduction

Primarily motivated by climate change concerns, the interest in biogas sharply increased in the new millennia. Global biogas production has more than quadrupled since 2000, with Europe leading the global race and accounting for a >50% share worldwide [1]. The EU's biogas production doubled between 2008 and 2016, and despite slowing down since (increased by just 3% from 2016 to 2019), an additional doubling until 2030 is foreseen [2,3]. About 90% of the biogas production is used for power and heat cogeneration

(CHP), although biogas upgrading to bio-methane for transportation fuel or injection to the natural gas networks is gaining an increasing share [4]. Biogas-CHP mostly refers to decentralized plants, in which the produced biogas is cleaned and directly fed to on-site ICEs, of 30–40% electrical efficiency [4–8].

Solid oxide fuel cells (SOFCs) exhibit the advantage of uniquely high efficiencies (50–60% or even >60% when combined with down-streaming turbines) compared to ICEs, and they can ideally replace ICEs in biogas-CHP plants [5,7,9–11]. Compared to the technologically more mature proton exchanging membrane fuel cells (PEMFCs), of considerably lower cost (about one third of the SOFCs) and lower efficiency (<50%), which operate at low temperatures (<100 °C) and require a complicated system of sequential catalytic reactors for CO/CO_2 elimination and biogas conversion to pure hydrogen [5], SOFCs have advantages such as remarkably higher efficiencies, being fuel flexible (they utilize CO and even dry CH_4 as fuels), withstanding the presence of CO_2 up to high percentages [12] and operating at high temperatures (~800 °C), which allow the utilization of the residual high-quality heat and the unburned fuel in the downstream gas and/or steam turbine for additional power generation [5]. Moreover, SOFCs bypass the disadvantages of corrosive electrolytes and CO_2 recycling complexities of the molten carbonate fuel cells (MCFCs), which are technologically less mature and also operate at high temperatures [13–15]. Nonetheless, an SOFC's high investment cost, currently at 7500–10,000 EUR·kWe^{-1} [16], compared to <1500 EUR·kWe^{-1} for ICEs or even the <2000 EUR·kWe^{-1} for PEM fuel cells, renders their use economically ineffective. Moreover, the replacement of ICEs by SOFC units would require additional and advanced biogas cleaning [7,17], as well as biogas partial reforming to enhance the SOFC's performance and to prevent thermal stressing and SOFC degradation due to carbon deposition [18].

The biogas-SOFC research has been ongoing for more than 20 years [9,19–21]. SOFCs' operation on biogas along with their potential utilization for biogas-CHP have been extensively studied, and the relevant research has been repeatedly reviewed [5,18]. The relevant research has focused on SOFCs' operating conditions [22], biogas pre-reforming [23], the impurities effect on the activity of the anode [24–26] and prototype testing [12,27,28], including the combined processes of artificial biogas desulfurization, pre-reforming and SOFC short stacks [29]. The CO_2 content of biogas is generally considered to assist the internal reforming of its CH_4 content within the SOFC's anode and to only slightly affect the SOFC's performance [9,19,27,30,31].

In parallel, considerable research efforts have been devoted to the modelling of biogas-fed SOFCs, predicting electrical efficiencies that range between 35 and 50% of the biogases' Lower Heating Values (LHVs), depending upon the SOFCs' operation point, the assumed fuel utilization and the biogas partial conversion to H_2, prior to its supply to the SOFC [9,20,32,33]. For integrated biogas-SOFC systems, as the one examined herein, which combine SOFC units with biogases' pre-reforming, thermally sustained by the SOFC's high-quality heat recycling, and down streaming gas or steam turbines for additional power generation, electrical efficiencies of up to 60 [20,30,33] or even 70% [10] have been reported depending upon the extent of biogas pre-reforming, the SOFC's efficiency, the extent of fuel utilization within the SOFC, the unburned fuel combustion, the type of downstream process for additional power generation and other parameters [5].

Based upon the accumulated lab-scale research on artificial biogas as well as on biogas-SOFCs and integrated process simulations, biogas-SOFC research has already reached demonstration level in pilot and real-scale plants [34–38]. The BIOCELL project studied the performance of a 2.8 kWe biogas-SOFC integrated process, including the effective removal of sulphur and pre-reforming. Optimized so as to meet the heat requirements of biogas generation, the overall electrical efficiency was reported at 34% [34]. The DEMOSOFC project installed and operated an industrial scale 174 kWel SOFC unit at a waste water treatment plant (WWTP), and illustrated the technical feasibility of SOFC systems operating on biogas with increased efficiency (50–55% electrical efficiency and 80–90% cogeneration efficiency) and reduced emissions [36,38,39]. The biogas-SOFC integrated process did not

involve biogas pre-reforming and focused on the deep and reliable removal of biogas contaminants [36]. The obtained efficiencies were independent of biogas CH_4 content and constantly high, whereas the SOFC operation could cope with the WWTP's power demand variations [38].

Despite the ongoing intense research and the escalation of this research to biogas-SOFC demonstration projects, only a few efforts have dealt with the economics of biogas-SOFC solutions. These efforts recognize the SOFC unit investment cost, as well as the investment cost of the required advanced biogas cleaning, as the most important challenges for the economic competitiveness of the biogas-SOFC plants, compared to the established biogas-CHP with ICE [5]. For small biogas-CHP plants of 33 $m^3 \cdot h^{-1}$ biogas production (~65 kWe for ICE-CHP capacity, increased to ~90 kWe for SOFC-CHP), Gandiglio et al. performed an economic comparison between distributed biogas-CHP with traditional ICEs and highly efficient CHP with SOFCs. The drastic increase in the electric efficiency, from 38 to 53%, translated into higher annual incomes for the SOFC-CHP; although this was based upon significantly increased investment. Assuming 200 $EUR \cdot kWe^{-1}$ capital cost for the traditional biogas cleaning to ICE specifications and 1000 $EUR \cdot kWe^{-1}$ for the advanced biogas cleaning to SOFC specifications, as well as near future SOFC costs at 3000–5000 $EUR \cdot kWe^{-1}$ compared to 1500 $EUR \cdot kWe^{-1}$ for ICEs, they reported investment Pay Back Times (PBT) that increased from <2 years for ICE-CHP to 3.5 and 7 years for SOFC-CHP (depending upon SOFC cost), for a 280 $EUR \cdot MWh^{-1}$ subsidized bio-electricity price [40]. The same research group, for the same subsidized bio-electricity price and SOFC costs variating between 3000–5000 $EUR \cdot kWe^{-1}$, depending upon the plant's capacity (13–500 $m^3 \cdot h^{-1}$ biogas production), compared to 1500 $EUR \cdot kWe^{-1}$ for ICE, reported PBTs that increased from 3–4 years for ICE-CHP to 9–11 years for SOFC-CHP, decreasing with the plant's capacity. The investment cost of the SOFC that required advanced biogas clean-up was regarded as 300–400 $EUR \cdot kWe^{-1}$, compared to 175–200 $EUR \cdot kWe^{-1}$ for ICEs. They also proposed biogas upgrading to bio-methane, as an alternative to pre-reforming, which could substantially improve economics, provided that the SOFCs' degradation rate remained below 0.02%·1000 h^{-1} [41]. Papadias et al. [42] estimated that a fuel cell system cost, with advanced biogas cleaning, in the range of 4000–4500 $EUR \cdot kW^{-1}$ could lead to positive internal rates of return on investment (IRRs) and become competitive with the regular biogas-CHP with ICEs, with a 120 $EUR \cdot kWh^{-1}$ electricity price. The advanced biogas cleaning system, for the practical elimination of H_2S and siloxanes, accounted for about 20% of the total equipment cost. Trendewicz and Braun [43] studied the effect of a biogas-SOFC plant's capacity on its economic prospects. They estimated the SOFC-CHP installation cost to de-escalate from 6500 to 4000 $EUR \cdot kW^{-1}$ with the plant capacity increasing from 640 to 11,920 kW of biogas LHV at the inlet, and to become economically competitive with the established biogas-CHP systems, with electricity prices at about 120 $EUR \cdot kWh^{-1}$. The SOFC unit area specific cost was regarded as being 1820 $EUR \cdot m^{-2}$, and the plant's electrical efficiency was estimated at 52% of biogas LHV. The costs of the SOFC unit and of the biogas advanced cleaning system accounted for 27–44% and 23–25%, respectively, of the CHP equipment cost, the first escalating with the plant's capacity, as a result of the modular nature of the SOFC technology. Provided that the SOFC specific cost drops adequately, to estimated values below 3500 $€ \cdot kW^{-1}$, so the biogas-SOFC CHP solution's propagation could become market-driven and without state-induced incentives, the overall installed SOFC capacity, just in the niche sector of wastewater treatment, can exceed 1300 MW [44,45]. Nonetheless, these efforts have not tackled the issue of the economically optimum sizing of the SOFC unit, with respect to its operational point, nor the issue of the appropriate economic feasibility criteria, to validate the economic performance of biogas-SOFC CHP.

In this context, and aiming to contribute to the crucial aspects that have not yet been tackled by the literature regarding the economic evaluation of the biogas-SOFC options, the present study assesses the economic feasibility of biogas-SOFC CHP, by the direct comparison of its economic performance with the conventional ICE-based biogas cogeneration, under the same assumptions. Thus, as well as the core issues of: (i) the

SOFCs high investment cost that hinders their application despite their high efficiency, and (ii) the process scale effect on economics, which have already been issued in the literature; the present investigation also focused on: (iii) the sizing of the employed SOFC unit, with respect to its operational point, i.e., for the biogas-SOFC integrated plant to either implement a small SOFC unit of lower cost, to operate at its maximum power density and low efficiency, or a larger and more expensive SOFC unit, to operate at lower power density and higher efficiency, (iv) the effect of the economic feasibility criteria used to assess the economics, on the economic assessment itself, and (v) the effect of economic feasibility criteria on the optimization of the employed SOFC size. Regarding the latter, the IRR criterion, which pays more attention to the initial investment, tends to charge poorer economic performance to the biogas-SOFC CHP due to its considerably higher initial investment, compared to the conventional biogas-CHP with ICEs. Consequently, it should be expected to optimize this performance for smaller SOFC units of lower cost and efficiency. On the other hand, the NPV criterion, which pays more attention to the annual profitability, should be expected to optimize the biogas-SOFC plant's economic performance for larger SOFC units of higher efficiency, despite their higher cost, whereas the NPV-based PBT should be expected to compromise this effect because it calculates profitability for a shorter time period. The study was based upon the simulation of a biogas-SOFC integrated system and the economics of biogas plants, according to the specified Excel Calculation Tool for Economic Analysis of Biogas Plants (Biogas Plants Calculation Tool—BPCT) of the Big-East project that was used [46].

2. Methodology

The overall methodology was to design, thermodynamically simulate and cost a SOFC-based CHP process, for two distinct cases of biogas supply rate (250 and 750 m$^3 \cdot$h^{-1}). These SOFC-CHP processes were considered to substitute the conventional ICE-CHP systems of two regular biogas-CHP plants of the aforementioned biogas capacities. The BPCT tool of the Big-East project [46] breaks down the initial investment of conventional biogas plants, and allows the substitution of the performance characteristics (efficiency and power generation) and the cost of the ICE-CHP system, which is initially incorporated in the tool, by the performance characteristics and the cost of the simulated SOFC-CHP system. The same tool calculates the depreciated annual operation expenses as well as the depreciated annual revenues, according to an externally defined discount rate, set by the BPCT tool to the typical value of 5.5%. Based upon the BPCT-calculated depreciated annual revenues of both the biogas-ICE and the biogas-SOFC CHP plants, throughout the plants' lifetime (regarded at 15 years), the economic performance of both the ICE and the SOFC biogas-CHP options, at the aforementioned capacities, was evaluated by the economic criteria of the Internal Rate of Return (IRR), the Net Present Value (NPV) and the Pay Back Time (PBT). For the biogas-SOFC CHP plants of either 250 or 750 m$^3 \cdot$h^{-1} biogas capacity, SOFC units of variable sizes (i.e., of variable surface areas) and costs were considered, so the employed SOFC units were able to operate at variable efficiencies and power outputs.

2.1. System Description and Process Simulation

The integrated SOFC-based CHP process is shown in Figure 1 and includes:

- additional biogas purification, with respect to the purification required for diesel engine biogas-CHP;
- a biogas and an air blower;
- the biogas pre-reformer with incorporated heat exchange, utilizing a part of the anode's exhaust, for the partial CH$_4$ conversion to H$_2$;
- the SOFC fuel cell system, including system balancing and power conditioning;
- a preheater for the cathodic air supply;
- an afterburner, for the complete combustion of the remaining fuel agents, that exit the SOFC's anode unburnt;
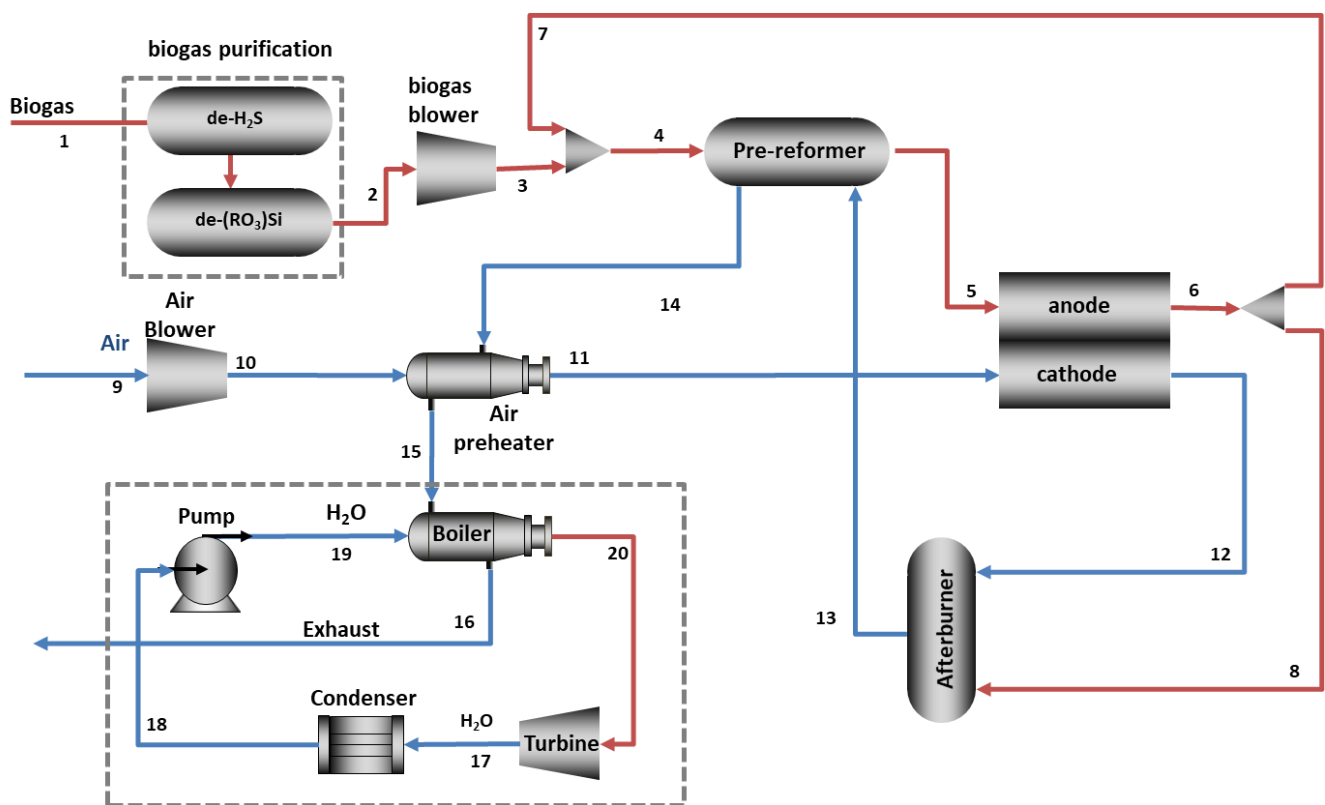- a steam turbine unit, for additional electricity generation.

Figure 1. Scheme of the proposed cogeneration process using SOFC cell.

Biogas of typical composition (Stream 1) is purified (Stream 2), slightly compressed (Stream 3) and mixed with the 50%v of the anode's exhaust gases (Stream 7), which are rich in steam and at high temperature (800 °C), and directly utilized as the reforming agent. The mixture (Stream 4) is then fed to a catalytic reformer, where 66.8% of the biogas' CH_4 is converted to H_2 and carbon dioxide, still at 800 °C. The heat required to maintain a constant temperature at the pre-reformer is provided by the hot exhaust gases of the afterburner (Stream 13).

The pre-reformed fuel (Stream 5) is fed to the anode of the fuel cell, the cathode of which is supplied with preheated air (Stream 11). The cell operation temperature is set to 800 °C, with a typical fuel utilization factor (U_f) of 80% [43]. The anode's exhaust gases (Stream 6) are partially (50% v) recycled to the pre-reformer (Stream 7) and the rest (Stream 8) are catalytically burned in the afterburner, with the cathode's depleted air (Stream 12). The burner's exhaust (Stream 13) is used to supply heat at the pre-reformer and the air preheater (Stream 14), while the remaining high-quality heat is supplied to the steam turbine (Stream 15). In the steam turbine, the after-burner's exhaust gases generate superheated steam at 40 bars, which condensates at 0.6 bars, to generate low-quality heat for the anaerobic digester and potentially other uses. The pressure drops, regarded for the individual components of the process, are given in Table 1.

Table 1. Pressure drops in the biogas-SOFC process components [43].

System Component	ΔP (kPa)
fuel purification unit	0.10
pre-reformer (fuel stream/heat exchanger stream)	0.02/0.02
stack (anode/cathode)	0.02/0.07
air preheater (air stream/exhaust gases stream)	0.05/0.05
afterburner	0.02
boiler	0.05

Two distinct cases of biogas supply (250 and 750 $m^3 \cdot h^{-1}$) were examined. In both cases, the operation of the integrated process was investigated for a range of SOFC units of variable surface areas. For the aforementioned biogas supply rates and a given fuel utilization (i.e., for constant fuel consumption and total current), the alteration of the SOFC's surface area (i.e., of its size and cost) alternates its current density and the operation potential, as well as the SOFC's power generation and efficiency. This alteration also affects the heat duty of the cathode preheater and the residual heat supply to the steam turbine.

The operational features (streams' temperatures, pressures, compositions and flowrates) of the biogas-SOFC CHP system of Figure 1, for the minimum examined SOFC size, which corresponds at SOFC's operation at maximum power density, are presented in Table 2. Temperatures at the exits of the air preheater (Streams 11 and 15) variate with the employed SOFC unit size and electric efficiency, affecting the steam temperature (Stream 20) and its flowrate, as denoted in Table 2. The pattern for the thermodynamic calculations of the involved processes is presented in Appendix A.

Table 2. Flowrates, molar fractions and operational conditions of the biogas-SOFC CHP system of Figure 1, for SOFC operation at maximum power density.

Stream	1	2	3	4	5	6	7	8	9	10
P, bar	1.01	0.91	1.19	1.19	1.17	1.15	1.15	1.15	1.01	1.27
T, °C	37.0	37.0	56.7	555.3	800	800	800	800	25.0	50.9
Y_{CH4}, %	60.00	60.15	60.15	18.80	4.99	-	-	-	-	-
Y_{CO2}, %	35.91	36.00	36.00	41.31	43.10	43.72	43.72	43.72	0.04	0.04
Y_{H2}, %	0.50	0.50	0.50	8.50	46.78	12.14	12.14	12.14	-	-
Y_{H2O}, %	2.34	2.35	2.35	30.91	4.87	43.90	43.90	43.90	1.28	1.28
Y_{N2}, %	0.50	0.50	0.50	0.32	0.26	0.24	0.24	0.24	77.81	77.81
Y_{O2}, %	0.50	0.50	0.50	0.16	-	-	-	-	20.87	20.87
Y_{Ar}, %	-	-	-	-	-	-	-	-	0.09	0.09
V_{250} [1], $m^3 \cdot h^{-1}$	284.0	314.3	255.9	2055.7	3385.7	3788.1	1894.0	1894.0	8334.8	7209.5
V_{750} [1], $m^3 \cdot h^{-1}$	852.1	943.0	767.6	6167.2	10,157.0	11,364.2	5682.1	5682.1	25,004.4	21,628.4
Stream	11	12	13	14	15	16	17	18	19	20
P, bar	1.22	1.15	1.13	1.11	1.06	1.01	0.60	0.60	40.00	40.00
T, °C	504.6 [2]	800	860.2	755.8	388.20 [3]	120.0	85.5	85.5	86.8	328.2 [4]
Y_{CH4}, %	-	-	-	-	-	-	-	-	-	-
Y_{CO2}, %	0.04	0.04	3.08	3.08	3.08	3.08	-	-	-	-
Y_{H2}, %	-	-	-	-	-	-	-	-	-	-
Y_{H2O}, %	1.28	1.32	5.14	5.14	5.14	5.14	100.00 [5]	100.00 [6]	100.00 [6]	100.00 [7]
Y_{N2}, %	77.81	80.63	75.37	75.37	75.37	75.37	-	-	-	-
Y_{O2}, %	20.87	18.01	16.41	16.41	16.41	16.41	-	-	-	-
Y_{Ar}, %	0.09	0.10	0.09	0.09	0.09	0.09	-	-	-	-
V_{250} [1], $m^3 \cdot h^{-1}$	18,009.5	25,438.7	29,253.1	27,034.4	18,193.3	11,349.0	39.4	0.02	0.02	1.06 [8]
V_{750} [1], $m^3 \cdot h^{-1}$	54,028.6	76,316.0	87,759.2	81,103.3	54,579.9	34,047.0	118.1	0.05	0.05	3.17 [9]

[1] Volumetric flows for the cases of 250 and 750 $m^3 \cdot h^{-1}$ STP. [2] Increases to 616.9 °C with the increase in the SOFC's area. [3] Decreases to 276.1 °C with the increase in the SOFC's area. [4] Decreases to 256.1 °C with the increase in the SOFC's area. [5] Water/steam mixture of biogas production. [6] Liquid water. [7] Superheated steam. [8] Decreases to 0.87 $m^3 \cdot h^{-1}$ with the increase in the SOFC's area. [9] Decreases to 2.62 $m^3 \cdot h^{-1}$ with the increase in the SOFC's area.

2.1.1. Biogas Production

In order to determine the operational characteristics of the low solids (5%), mesophilic anaerobic digester for biogas production, the Excel Calculation Tool for Economic Analysis of Biogas Plants (Biogas Plants Calculation Tool—BPCT) of the Big-East project was used [46]. For the simulation needs, a typical average biogas composition was considered (Table 3), which is in agreement with the typical biogas composition of the BPCT. A 60/40%w mixture of cattle waste and energy silage (silage maize) was considered as the raw biomass feedstock. Based upon the BPCT's assumptions, 14,440 $tn \cdot yr^{-1}$ of cattle waste (10% TS, specific biogas production: 25 $m^3 \cdot tn^{-1}$) and 9626 $tn \cdot yr^{-1}$ of energy silage (32% TS, specific biogas production: 190 $m^3 \cdot tn^{-1}$) were fed to the digester, for the production of 250 $m^3 \cdot h^{-1}$ of biogas with CH_4/CO_2 = 60/40%v composition, and 43,319 $tn \cdot yr^{-1}$ of cattle waste and 28,879 $tn \cdot yr^{-1}$ of energy silage, for the production of 750 $m^3 \cdot h^{-1}$ of biogas, of the same composition. For conventional power generation in an ICE of 40% electric and 88% cogeneration efficiency, the aforementioned capacities corresponded to electric

power generations of 600 and 1800 kW, respectively. According to the same tool, 30% of the generated heat and 7% of the generated electricity were consumed in the unit itself. Thus, the available electric power was 558 and 1674 kW, in the two cases, while the available thermal power was 504 and 1512 kW, respectively [46].

Table 3. Biogas composition, % [47].

CH$_4$	CO$_2$	H$_2$O	N$_2$	H$_2$S	NH$_3$	O$_2$	H$_2$
60.00	35.91	2.34	0.50	0.20	0.05	0.50	0.50

Typical harmful impurities of biogas refer to H$_2$S and siloxanes. H$_2$S requires removal due to its corrosive nature, and if fed to a SOFC system, it poisons the nickel catalyst, which is present in both the pre-reformer and the anode [47]. For the safe operation of the SOFC unit, the H$_2$S concentration must be maintained below 0.2 ppm [48]. Siloxanes are highly volatile, organic compounds that oxidize to SiO$_2$ glassy deposits and they are particularly dangerous in high temperature fuel cells, as they can fill the porous structure of the anode [49]. The concentration of siloxanes in the biogas for fuel cell applications must remain below 3 ppm.

Thus, biogas purification usually involves the successive steps of desulphurisation and desiloxanation. Regarding siloxanes, their concentration after purification was considered negligible, while the concentration of H$_2$S after desulphurisation was considered equal to the biogas feed specification for SOFCs, i.e., 0.2 ppm [43]. At the outlet of the purification processes, cleaned biogas was considered to be 37 °C (i.e., at the temperature of the mesophilic anaerobic digester) and 91 kPa (i.e., 10 kPa below the pressure of the atmospheric digester—Table 1).

2.1.2. Biogas Pre-Reformer

Pre-reformers are widely used in SOFC systems, in order to partially convert CH$_4$ to H$_2$ and CO$_2$, prior the fuel cell, and thus to prevent carbon deposition at the anode as well as to balance local thermal gradients within the cell [50–52]. Exhaust gas recirculation to the pre-reformer is a common practice for fuel cell systems' design [43]. The benefits associated with this option have to do with the use of the high temperature steam generated at the anode, which bypasses the necessities for an additional steamer/superheater as well as for the consumption of fresh water. For the simulation of the pre-reformer, a typical operation temperature (800 °C [53]) was considered, and the overall reaction:

$$CH_4 + 2\,H_2O \leftrightarrow CO_2 + 4\,H_2 \tag{1}$$
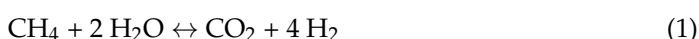
was assumed to reach the equilibrium at this temperature. The partial recycle of the anode's exhaust gas was used as the reforming agent consisting of 43.7% CO$_2$, 43.9% H$_2$O, 12.1% H$_2$ and minor amounts of N$_2$. To prevent carbon deposition on the nickel catalyst of the pre-reformer, through the Boudouard equilibrium:

$$CO_2 + C \leftrightarrow 2\,CO \tag{2}$$

the steam to carbon ratio (S/C) ratio:

$$S/C = \frac{n_{H_2O}}{n_{CH_4} + n_{CO_2}} \tag{3}$$

(n_{H2O}, n_{CH4} and n_{CO2} are the corresponding molar flowrates at the reformer's inlet) should be greater than 0.46, at 800 °C [53]. The CO$_2$ content of both the biogas and the reforming agent shifts forward the Boudouard equilibrium; thus, less steam is required to ensure carbon-safe operating conditions [50], whereas the increase in S/C decreases the overall electrical efficiency of biogas-SOFC processes [43]. In view of the above, a 50% recycle ratio

of the anode's exhaust was selected as the reforming agent, resulting in a 0.51 S/C, i.e., ~10% higher than the minimum safety threshold.

The thermodynamically calculated equilibrium constant K of Reaction 1:

$$K = \exp\left(\frac{-\Delta G_{reaction2}}{RT}\right) \tag{4}$$

at the pre-reformer's temperature, resulted in a 66.8% CH_4 conversion in both cases of 250 and 750 $m^3 \cdot h^{-1}$ biogas supply, which is in accordance to relevant literature [54].

2.1.3. SOFC

A typical anode-supported planar SOFC was regarded for the simulation, and it was set to operate at the typical temperature of 800 °C [53]. The remaining CH_4 in the pre-reformed biogas (Stream 5), was assumed to be totally converted to additional H_2, through Reaction 1, within the SOFC's anode. This was due to H_2 consumption at the anode, as well as the progressive steam generation by H_2 combustion, that further shift the equilibrium of Reaction 1. Thus, the fuel utilization (U_f) at the SOFC was regarded at 80% of the total H_2 fed to its anode, i.e., the molecular H_2 at the anode's inlet and the H_2 that is stoichiometrically generated within the anode by the internal reforming of CH_4.

Preheated air, composition shown in Table 4, was supplied to the SOFC's cathode. The air supply to the cathode was set accordingly, so that the depleted air exited the cathode with 18% O_2. The air supply to the cathode was calculated at 9789.8 and 29,231.0 $kg \cdot h^{-1}$ for 250 and 750 $m^3 \cdot h^{-1}$ biogas supply, respectively.

Table 4. Assumed air composition, %.

N_2	O_2	CO_2	H_2O	Ar
77.81	20.87	0.04	1.28	0.093

For the operating potential of the SOFC:

$$V_{cell} = E - n_{act} - n_{ohm} - n_{conc} \qquad [V] \tag{5}$$

(E is open circuit voltage (OCV) at the operating conditions and n_{act}, n_{ohm}, n_{conc} stand for the activation, the ohmic and the concentration overpotentials, respectively (n_{conc} was regarded negligible, for SOFC operation near its nominal power output), E was calculated by the Nernst Equation [55]:

$$E = E^o + \frac{RT}{4F} \ln \frac{Y_{aveH2,an}}{Y_{aveH2O,an} \times Y_{aveO2,cath}^{0.5}} \qquad [V] \tag{6}$$

where E^o is the OCV at standard conditions (1.185 V), and the molar fractions $Y_{aveH2,an}$, $Y_{aveO2,cath}$ and $Y_{aveH2O,an}$ were calculated as the mean values, between the inlet and the outlet of the anode or cathode, respectively. The activation overpotential was calculated as [55]:

$$n_{act} = i \times (R_{act,an} + R_{act,cath}) \qquad [V] \tag{7}$$

where i is the cell's current density ($A \cdot m^{-2}$) and $R_{act,an}/R_{act,cath}$ the activation resistances of the anode/cathode, respectively [55]:

$$R_{act,an} = \frac{R \times T}{D_{an} \times n \times F \times (Y_{H_2})^{m_{an}} \times \exp\left(\frac{-E_{an}}{RT}\right)} \qquad [\Omega \cdot m^2] \tag{8}$$

$$R_{act,cath} = \frac{R \times T}{D_{cath} \times n \times F \times (Y_{O_2})^{m_{cath}} \times \exp\left(\frac{-E_{cath}}{RT}\right)} \qquad [\Omega \cdot m^2] \tag{9}$$

The D_{an}/D_{cath}, m_{an}/m_{cath} and E_{an}/E_{cath} coefficients are given in Table 5, for the regarded anode (Ni/YSZ cermet) and cathode (LSM/YSZ cermet), respectively. For the assumed constant U_f, the activation resistances remained constant, at $R_{act,an} = 6.41 \times 10^{-5}$ $\Omega \cdot m^2$ and $R_{act,cath} = 1.36 \times 10^{-5}$ $\Omega \cdot m^2$, regardless the biogas supply rate or the SOFC's surface area.

Table 5. Constants for activation resistances calculation [55].

D_{an}	2.13×10^{-8}	$A \cdot m^{-2}$	m_{an}	0.25	E_{an}	110,000	$J \cdot mol^{-1}$
D_{cath}	1.49×10^{11}	$A \cdot m^{-2}$	m_{cath}	0.25	E_{cath}	160,000	$J \cdot mol^{-1}$

The SOFC's ohmic overpotential n_{ohm} was calculated by the specific ohmic resistances ρ_i of the employed components [56]:

$$\rho_i = A_i \times \exp\left(\frac{B_i}{T}\right) \quad [\Omega m] \tag{10}$$

(subscript i refers to the Ni/YSZ anode, the LSM/YSZ cathode, the YSZ electrolyte and the $LaCrO_3$ current collector), where i represents cell's current density ($A \cdot m^{-2}$) and A_i, B_i, l_i are given in Table 6. The ohmic overpotential of the cell was calculated as [56]:

$$n_{ohm} = i \sum \rho_i \frac{l_i}{S_i} \quad [V] \tag{11}$$

with l_i and s_i standing for the thickness and the surface area of each individual component, respectively, and varied with the SOFC's surface area.

Table 6. Constants for the ohmic resistances calculation [56].

	A_i, Ωm	β_i, K	l_i, μm	ρ_i, Ωm
YSZ	0.0000029	10,350	50	1.876×10^{-10}
Ni/YSZ	0.000003	1392	545	8.198×10^{-7}
LSM/YSZ	0.0000081	−600	400	1.417×10^{-5}
LaCrO3	0.001256	−469	100	9.937×10^{-2}

The total current of the cell was constant for each one of the two cases of biogas supply, and was calculated by the relation:

$$I = 2 \times F \times F_{O^{2-}} \quad [A] \tag{12}$$

where $F_{O^{2-}}$ stands for the O^{2-} anions' supply to the anode ($mol \cdot sec^{-1}$), which was stoichiometrically determined by the anodic H_2 consumption and F is the Faraday's constant (96.484 $cb \cdot mol^{-1}$). The current density is given by:

$$i = \frac{I}{A_{cell}} \quad [A \cdot m^{-2}] \tag{13}$$

where A_{cell} is the apparent surface area (m^2) of the cell, and the overall electrical power generated by the cell was calculated as:

$$P = V_{cell} \times I \quad [W] \tag{14}$$

As mentioned previously, the performance and the economics of the integrated process were studied for SOFC units of different surface areas (i.e., for SOFCs of different size and cost), regarding each one of the examined biogas feeds. For constant total current (determined by the biogas feed and the constant U_f), these surface areas were selected accordingly, so that for the SOFCs to operate at or below their maximum power density

(MPD), i.e., for current densities lower than the current density at the MPD. At this operational region, the decrease in the current density increased the SOFCs' efficiency and power output, but decreased the residual heat for the steam turbine. The overall efficiency of the cell was defined as:

$$\eta_{SOFC} = \frac{W_{SOFC}}{LHV_{H2}} \times 100 \ [\%] \tag{15}$$

where W_{SOFC} stands for the electrical power generated by the SOFC and LHV_{H2} for the Lower Heating Value of the H_2 consumed at the anode.

2.1.4. Afterburner

A catalytic afterburner was used to totally combust the remaining fuel components of the part of the SOFC's anode exhaust gases that was not recycled to the pre-reformer. The depleted air from the SOFC's cathode was used for the combustion, corresponding to a vast oxygen excess of about 4000%, with respect to the H_2 fuel supplied to the afterburner. The temperature at the outlet of the afterburner was calculated at 860.1 °C, by its energy balance.

2.1.5. Steam Turbine

A steam turbine was employed for the supplementary power generation by the residual high-quality heat of the process. Exhaust gases from the cathode's air preheater enter the boiler of the steam turbine at 276.1–388.2 °C, depending upon the SOFC's surface area, and they were to set to vent the integrated process at 120 °C. Water enters the boiler as compressed liquid at 86.8 °C and exits as superheated steam at 40 bar. The steam turbine's condenser was set to operate at 60 kPa, in order to generate heat at an adequate temperature (88.3 °C), for the digester's heat requirements. The isentropic efficiencies of the turbine and the pump were assumed at 75 and 85%, respectively [57]. A part of the condenser's low-quality heat was used for the digester's thermal requirements, which were calculated by the BPCT at 216.0 and 648.0 kW, for the cases of 250 and 750 $m^3 \cdot h^{-1}$ biogas supply, respectively. The corresponding heat generation at the condenser was 277.2–543.4 kW for the 250 $m^3 \cdot h^{-1}$ case and 832.5–1588.7 kW for the 750 $m^3 \cdot h^{-1}$ case, decreasing with the SOFC's surface area.

2.1.6. Other Equipment (Blowers and Heat Exchangers)

The air blower increases the ambient air pressure to counterbalance the pressure drops at the air preheater's air stream (5 kPa), the fuel cell's cathode (7 kPa), the afterburner (2 kPa), the pre-reformer's exhaust gas stream (2 kPa), the air preheater's exhaust-gas stream (5 kPa) and the boiler (5 kPa) (Table 1). Thus, considering that ambient air enters the blower at 25 °C and 101.3 kPa, its duty was to increase this pressure to 127.3 kPa. Regarding 71.3% isentropic efficiency [43], the air blower power consumption was calculated at 72.2 kW for the case of 250 $m^3 \cdot h^{-1}$ biogas supply and 217.2 kW for the 750 $m^3 \cdot h^{-1}$ case (the outlet temperature was calculated at 50.9 °C).

The biogas blower aimed to overcome the pressure losses at the pre-reformer's fuel stream (2 kPa), the anode (2 kPa), the afterburner (2 kPa), the pre-reformer's exhaust-gas stream (2 kPa), the air preheater's exhaust-gas stream (5 kPa) and the boiler of the steam turbine (5 kPa). Assuming 101.3 kPa at the vent of the integrated process, the biogas blower should increase the biogas pressure from 91 to 119.3 kPa. Its isentropic efficiency was considered at 71.3% [43], and the electrical work consumed was calculated at 2.27 kW for the 250 $m^3 \cdot h^{-1}$ case and at 6.68 kW for the 750 $m^3 \cdot h^{-1}$ (the outlet temperature was calculated at 56.7 °C).

The air preheater (considered as a shell–tube heat exchanger) was employed to heat air from 50.9 °C to the temperature required for the SOFC's thermal balance. This temperature was calculated at 504.6 to 616.9 °C, increasing with the SOFC's surface area, regardless the biogas feed to the integrated process, due to the higher SOFC's overall power output at higher surface area, which decreases the SOFC generated heat, thus increasing its thermal requirements. The high temperature exhaust gases, after the pre-reformer, enter the air

preheater at 837.6 °C, regardless both the scale (i.e., the biogas supply rate) of the integrated process and the surface area of the employed SOFC. The latter is due to fact that, despite the decreased heat generation at larger SOFCs, this deficit is counterbalanced by the increased temperature of the cathodic air supply.

2.2. Cost Data

The total investment (I_T) of the conventional biogas plant with a CHP system based on ICEs was estimated by the correlation [58]:

$$I_T = 4.671 \times W_{el} - 0.92 \quad [\text{M€}] \tag{16}$$

where W_{el} is the net generated electrical power in kW. According to the BPCT calculation tool, the contribution of the individual cost elements to the total I_T is given in Table 7 [46]. This allocation allows the separated calculation of the CHP system. Thus, for the conventional CHP unit, the total I_T was calculated by Equation (16), whereas for the SOFC CHP system, the cost of the SOFC unit was separately calculated and added to the BPCT calculation tool to replace the cost of the conventional CHP system.

Table 7. Individual investment costs of the unit based on Standard Evaluation Sheet of CRES [46].

	% of I_T
Installation, buildings and site preparation	34.15
Machinery purchase	26.83
Electronic equipment	8.29
Project design and supervision	8.78
CHP system	21.95

The investment cost of the SOFC-based CHP system was calculated by the detailed costing of the Figure 1 equipment and systems, i.e., for:

1. the biogas cleaning system;
2. the biogas and the air blowers;
3. the air preheater;
4. the afterburner;
5. the pre-reformer;
6. the SOFC unit;
7. the steam turbine.

The costs of the biogas cleaning system (C_{CS}), the pre-reformer (C_{PR}) and the afterburner (C_{AF}) were calculated by correlations extracted from the relevant work of [43], based upon the Lower Heating Value of biogas (LHV_b (for the assumed biogas composition of Table 3, LHV_b = 21.49 MJ·m^{-3}, as calculated by the LHV of its CH_4 content) at the inlet of the process (values were converted to euros by the equivalence factor 0.922 EUR·\$$^{-1}$ and inflated from 2011 to 2022, assuming 2%·a^{-1} average inflation). Regarding the biogas cleaning system, C_{CS} was calculated by the correlation:

$$C_{CS} = 1091.6 \times \ln LHV_b - 6801.4 \quad [\text{kEUR}] \tag{17}$$

at 1434.9 and 2895.7 kEUR for 250 and 750 m^3·h^{-1} of biogas production, respectively. The pre-reformer cost was estimated by the correlation:

$$C_{PR} = 0.423 \times LHV_b^{0.672} \quad [\text{kEUR}] \tag{18}$$

at 74.39 kEUR for 250 m^3·h^{-1} biogas production and 155.72 kEUR for 750 m^3·h^{-1} biogas production, while the afterburner's cost was calculated by the correlation:

$$C_{AF} = 0.019 \times LHV_b^{1.001} \quad [\text{kEUR}] \tag{19}$$

at 37.23 and 112.87 kEUR for the two cases of biogas production, respectively.

The blowers and the air preheater costs were taken by the online Matches tool. For the blowers, this cost was based at the blowers' volumetric flowrate at its inlet, for rotary or centrifugal blower type [59], and for the biogas blower was estimated at 5.36 kEUR for 250 $m^3 \cdot h^{-1}$ biogas production and at 11.85 kEUR for 750 $m^3 \cdot h^{-1}$ biogas production. For the air blower, the corresponding costs were found at 80.82 and 96.75 kEUR, respectively. For the air preheater, the cost was estimated by the required heat exchange surface area (A_{PH}), for a shell–tube heat exchanger [60]. A_{PH} was calculated by the equation:

$$Q = U \times A \times \Delta T_{lm} \qquad [W/m^2] \qquad (20)$$

where Q is the heat transfer [W], as calculated from the process simulation, U is the total heat transfer coefficient, regarded at 30 $W \cdot m^{-2} \cdot K^{-1}$, and ΔT_{lm} is the mean logarithmic temperature difference:

$$\Delta T_{lm} = \frac{\Delta T1 - \Delta T2}{\ln \frac{\Delta T1}{\Delta T2}} \quad [K] \qquad (21)$$

($\Delta T_1 = T_{h1} - T_{c2}$ and $\Delta T_2 = T_{h2} - T_{c1}$, where 1 and 2 subscripts denote the inlet and outlet streams, h denotes the exhaust gas high temperature stream and c denotes the air low temperature stream), still calculated by the process simulation. The duty and, consequently, its size and cost of the air preheater varied with both the process's scale and the SOFC's surface area, in the ranges of 65.28–81.60 kEUR, for 250 $m^3 \cdot h^{-1}$ of biogas production and 95.34–118.29 kEUR, for 750 $m^3 \cdot h^{-1}$ of biogas production.

Regarding the SOFC unit cost, Hydrogen Europe Strategic Research and Innovation Agenda (SRIA) [16] targets a gradual cost reduction from about 10,000 $EUR \cdot kW_{el}^{-1}$ today, to 2000 $EUR \cdot kW_{el}^{-1}$ in 2030, for SOFC units >50 kW_{el}, whereas experts estimate further cost reduction to 1100 $EUR \cdot kW_{el}^{-1}$ in 2035, in a pathway towards a <2750 $EUR \cdot kW_{el}^{-1}$ in 2050 [11,61]. In this context, the SOFC unit cost was regarded at two distinct values, i.e., at 2000 and 1100 $EUR \cdot kW_{el}^{-1}$. These costs, referring to 2030 and 2035, respectively, corresponded to 5269 and 2898 $EUR \cdot m^{-2}$ of superficial surface area, for the calculated, by the present simulation, power density of 2.63 $kW \cdot m^{-2}$, at the maximum power point of SOFC's operation, which was in agreement with the relevant literature (biogas-fed SOFCs power density is reported at 207–273 $kW \cdot m^{-2}$ [5,43]).

The steam turbine's cost (C_{ST}) was calculated as for an integrated unit and based upon 0.6 escalation factor [62]:

$$C_{ST} = C\prime_{ST} \times \left(\frac{Q_{ST}}{Q\prime_{ST}} \right)^{0.6} \quad [EUR] \qquad (22)$$

where Q_{ST} (kW) is the steam turbine's capacity, expressed as heat supply at its inlet, and C^{ref}_{ST} (= EUR 27,989) is the reference cost for the reference heat supply of Q^{ref}_{ST} (= 15.1 kW) [63]. The cost of the steam turbine changes with the scale of the process (i.e., the biogas production), and with the SOFC size (i.e., the apparent surface of the cell), and varied from EUR 69.93–109.00 k for 250 $m^3 \cdot h^{-1}$ of biogas production and EUR 135.27–207.12 for 750 $m^3 \cdot h^{-1}$ of biogas production.

The indirect costs for the installation of the SOFC-CHP integrated process, including the engineering, the construction, the legal fees, etc., were considered at 37% of equipment/units cost [43].

The annual operating costs were calculated from the BPCT calculation tool [46], and referred to: (i) personnel cost (considered for one worker per installed 300 kWe, calculated at 25 $kEUR \cdot a^{-1}$ per worker and 50 $kEUR \cdot a^{-1}$ for administration cost), (ii) repair and maintenance of the biogas plant, excluding the CHP system (calculated at 2% of the buildings cost, 6% of machinery cost and 4% of electric equipment cost), (iii) repair and maintenance of CHP system, which was calculated at 0.010 $EUR \cdot kWh^{-1}$, for the conventional diesel-ICE system and 0.011 $EUR \cdot kWh^{-1}$, for the SOFC CHP process, including the SOFC stack replacement every five years [43], (iv) insurance costs accounted for 1% of the equipment and

units costs, (v) other operational costs, related to the biomass/manure handling (vehicles, personnel, lifters, etc.), which were regarded as 1.6 EUR·tn^{-1} the BPCT calculation tool [46], and (vi) the maize silage cost, which was regarded as 40 EUR·tn^{-1} [64] (manure biomass was regarded as zero cost). Operating costs, including maize silage, were inflated by an assumed average annual inflation of 2%·a^{-1}.

3. Results and Discussion

3.1. Process Performance

The calculated SOFC's operating potential and power density vs. current density are plotted in Figure 2a. For constant fuel utilization factor and constant fuel supply to the SOFC, for each one of the two process scales examined, the total electrical current of the cell is also constant (1274.1 and 3822.1 kA, for 250 and 750 m^3·h^{-1} biogas production, respectively). For constant total current, the current densities of Figure 2 correspond to different SOFC surface areas, i.e., to different SOFC sizes (and consequently costs). The SOFC surface areas, in order for the current density to variate in the examined range, are depicted in Figure 2b. These current densities also correspond to a range of power densities, from 70–100% of the SOFC's maximum power density (MPD), as denoted in parentheses in Figure 2. Thus, for the constant total current, in order for the SOFC to operate at 247.40–553.95 mA·cm^{-2} (1.84–2.63 kW·m^{-2}, that is 70–100% of the MPD, respectively) for both the examined biogas production capacities, its surface area should range from 230 to 515 m^2 for 250 m^3·h^{-1} biogas production, and from 710 to 1540 m^2 for 750 m^3·h^{-1} biogas production.
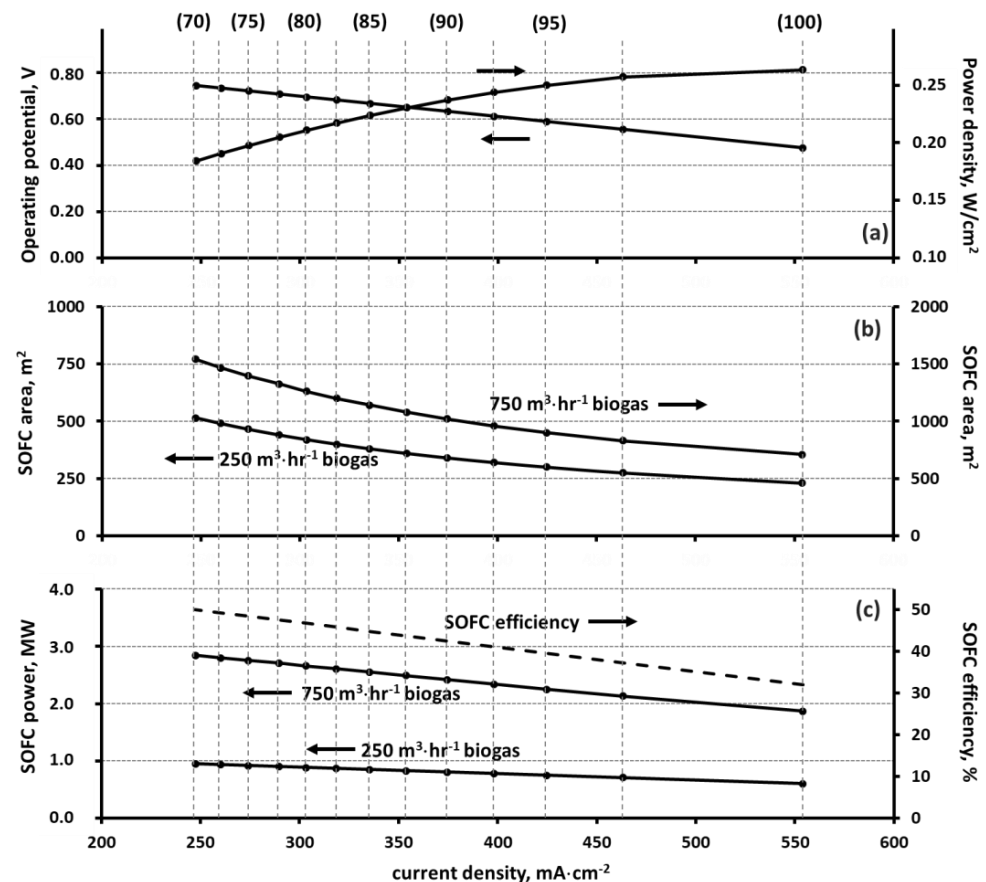

Figure 2. SOFC size and operation characteristics: (**a**) SOFC operation potential and power density (values in parentheses denote power density as percentage of the SOFC's maximum power density), (**b**) SOFC's surface area, and (**c**) SOFC efficiency and total power generation, for the two examined scales of the integrated plant.

The SOFC's efficiency (Equation (15)) does not depend on the overall biogas production and the scale of the integrated process, and increases as the current density decreases (Figure 2c). This results in increased total power generation for SOFC operation at lower current densities, i.e., for larger SOFC size and surface area, for each one of the two examined plant's capacities. Thus, for 250 $m^3 \cdot h^{-1}$ biogas production, a SOFC unit large enough to operate at 70% of its MPD (515 m^2 surface area), was calculated to generate 948.3 kW that decreased to 605.9 kW, for a SOFC unit adequately smaller, so as to operate at its MPD (230 m^2 surface area). The corresponding SOFC generation for the integrated biogas plant of 750 $m^3 \cdot h^{-1}$ biogas production was maximized at 2842.0 kW for the maximum examined SOFC's surface area of 1540 m^2 of maximum efficiency (50.1%) and minimum current density (247.40 $mA \cdot cm^{-2}$), and 1870.1 kW for 710 m^2 SOFC's surface area of minimum efficiency (32.0%) and maximum current density (553.95 $mA \cdot cm^{-2}$), respectively.

The SOFC's power generation (P_{SOFC}) increases with the cell area, whereas the steam turbine generated power decreases due to the higher SOFC's electrical efficiency, which reduces the residual high-quality heat of the integrated process, and consequently the available heat for power generation at the turbine (Figures 3 and 4). For both plant's capacities of 250 and 750 $m^3 \cdot h^{-1}$ biogas production, P_{SOFC} increases by 56.5%, by sizing the cell accordingly, so as to operate at 70% of its MPD, compared to a smaller cell, sized to operate at MPD (from 0.61 to 0.95 MW for the small plant and from 1.87 to 2.84 MW for the large plant, respectively). Conversely, the steam turbine-generated power (P_{ST}) decreases by 52.3% (from 0.15 to 0.07 MW for the small plant and from 0.42 to 0.21 MW for the large plant, respectively), for the same size variation in the employed SOFC, resulting in an overall increase in the total generated power (P_T) by 35.4% (from 0.75 to 1.02 MW for the small plant and from 2.29 to 3.05 MW for the large plant), and a 41.9% increase (from 0.635 to 0.901 MW for the small plant and from 1.941 to 2.701 MW for the large plant) in the net power production (P_{NET}), of the biogas-SOFC integrated process. P_{NET} refers to P_T minus the electricity consumption by the biogas production process and the blowers of the SOFC-based CHP system, of Figure 1, and it is the available power for the integrated plant to sell at 220 EUR$\cdot$MWh^{-1}.
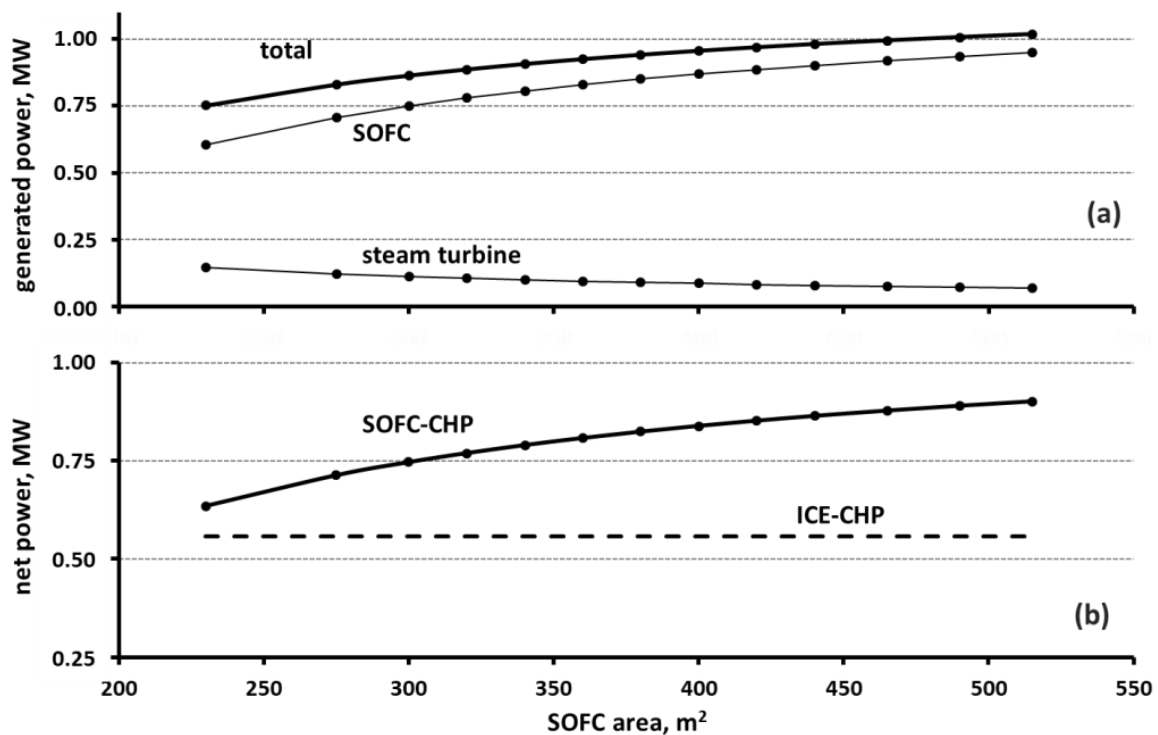

Figure 3. Biogas plant power generation and its dependence on the employed SOFC unit size, for 250 $m^3 \cdot h^{-1}$ biogas production.

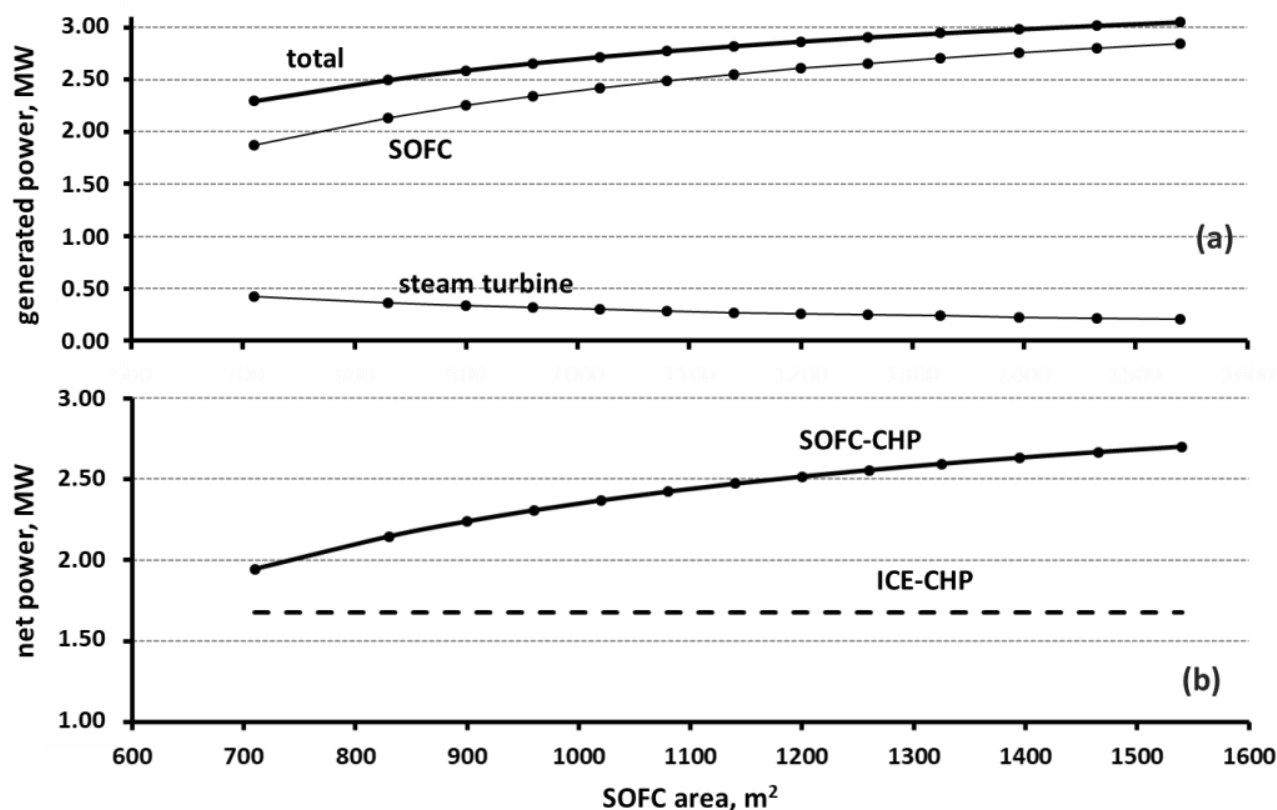**Figure 4.** Biogas plant power generation and its dependence on the employed SOFC unit size, for $750 \ m^3 \cdot h^{-1}$ biogas production.

Regarding the SOFC-based CHP, P_{NET} was computed to be 14–62% higher than the net power generation in a conventional ICE-CHP (i.e., P_{NET} = 0.635–0.901 MW, compared to the 0.558 MW by the conventional diesel engine, for $250 \ m^3 \cdot h^{-1}$ biogas production, and P_{NET} = 1.944–2.701 MW, compared to the 1.674 MW of the conventional ICE, for $750 \ m^3 \cdot h^{-1}$ biogas production). The available heat generation of the integrated process (i.e., the residual heat from the steam turbine minus the heat requirements of the anaerobic digestion for biogas production, which was regarded available for selling at 40 $EUR \cdot MWh^{-1}$) decreased with the employed SOFC size (from 0.33 to 0.06 MW for the $250 \ m^3 \cdot h^{-1}$ biogas production case, compared to 0.50 MW for ICE-CHP, and from 0.94 to 0.18 MW for the $750 \ m^3 \cdot h^{-1}$ case, compared to 1.51 MW for conventional CHP).

3.2. Cost of Investment and Operational Expenses

Due to the modularity of the SOFC technology and the constant values of the SOFC's area specific cost used herein, the SOFC unit cost is linearly proportional to its size. Comparing Figures 5a and 6a for the lower regarded SOFC area specific cost (1100 $EUR \cdot kW_{el}^{-1}$ or 2898 $€ \cdot m^{-2}$, foreseen for 2035), the total initial investment for the large capacity plant was 1.95–2.41 times higher than the total initial investment for a small capacity plant, this ratio decreasing with the employed SOFC size. For the higher regarded SOFC area specific cost, the total initial investment for the large plant was 2.50–2.62 times higher than that of the smaller. Notably, the net power generation (P_{NET}) of the large scale plant was 3.00 times higher than the net power generation of the small scale plant. This fact denotes the decrease in the specific investment cost, which reduces from 6.44–7.40 $kEUR \cdot kW_{el}^{-1}$ for the small plant to 5.39–5.82 $kEUR \cdot kW_{el}^{-1}$ for the large plant, regarding the low SOFC area specific cost, and from 8.29–8.58 $kEUR \cdot kW_{el}^{-1}$ for the small plant to 7.01–7.24 $kEUR \cdot kW_{el}^{-1}$ for the large plant, regarding the high SOFC area specific cost.
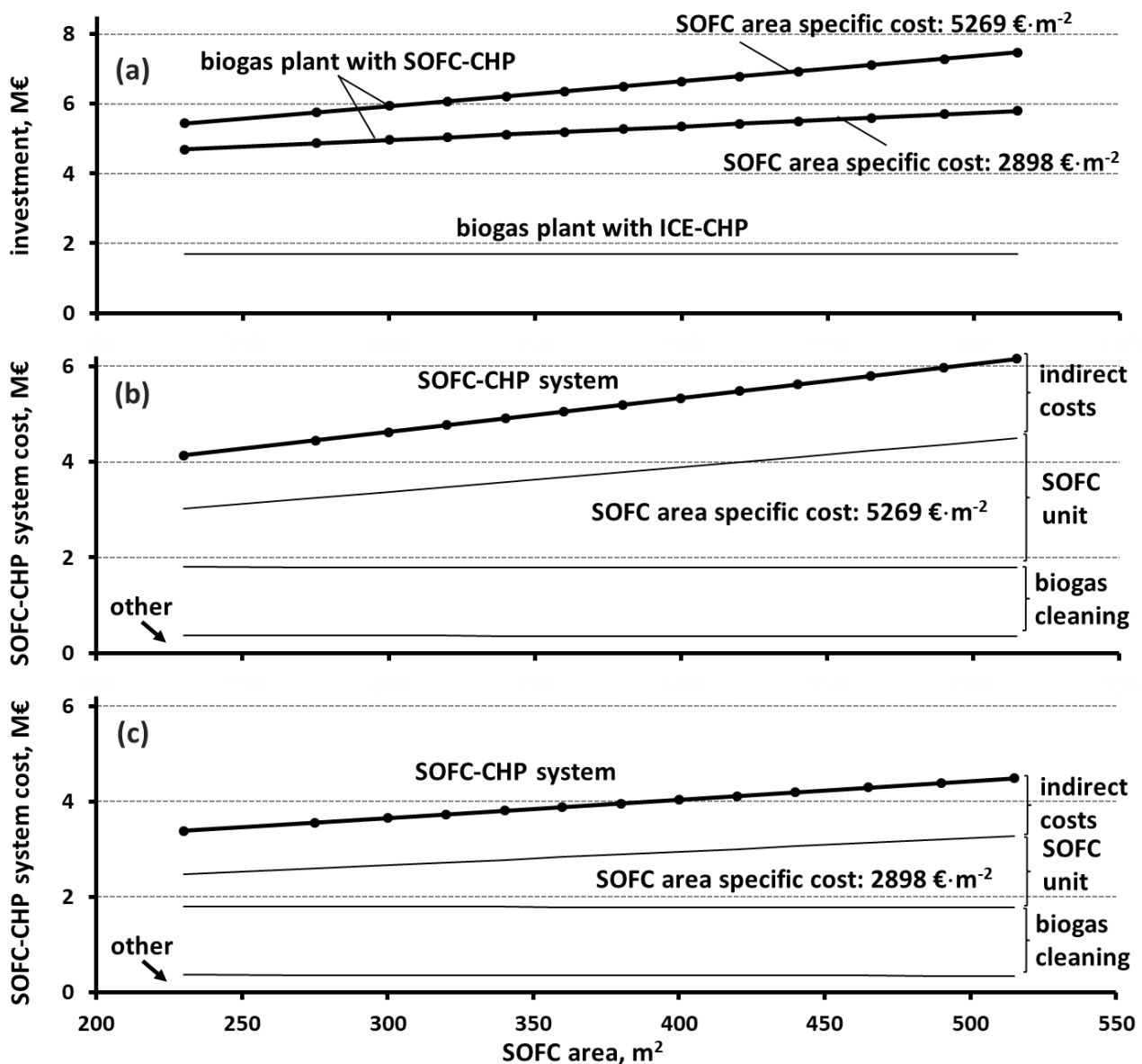
Figure 5. Initial investment of: (**a**) the conventional biogas-CHP plant with ICE-CHP, for 250 m$^3 \cdot$h^{-1} biogas production capacity, and of the corresponding SOFC-CHP system, for (**b**) 2898 EUR$\cdot$m^{-2} SOFC area specific cost and (**c**) 5269 EUR$\cdot$m^{-2} SOFC area specific cost.

For both the regarded area specific SOFC's costs, the overall initial investments of the biogas-SOFC integrated plants is significantly increased with the employed SOFC's size (Figures 5 and 6). Thus, for the minimal SOFC specific cost (2898 EUR$\cdot$m^{-2}) and for a SOFC unit of 230 m^2 surface area and 32.0% efficiency, operating at its maximum power density, the initial investment for the small scale biogas-SOFC plant was calculated to be 2.80 times higher than of the conventional ICE biogas-CHP plant (EUR 4.70 M compared to EUR 1.68 M). The overall electric efficiency of the SOFC-based plant was calculated at 45.2%, compared to the 40% of the conventional ICE biogas plant—Figure 5a. Still, for the minimum area specific SOFC cost of 2898 EUR$\cdot$m^{-2}, the employment of a much larger cell of 515 m^2 that operates at 70% of its maximum power density, with 50.6% SOFC efficiency and 63.0% plant efficiency, the initial investment of the SOFC-biogas plant was calculated to be 3.45 times higher than the conventional biogas plant. These factors increase from 2.80 to 3.24 and from 3.45 to 4.45 for the increased SOFC's specific cost projection to 2030 (2000 EUR$\cdot$kW$_{el}$$^{-1}$ or 5269 EUR$\cdot$m^{-2}). For the large scale biogas plant (750 m$^3 \cdot$h^{-1} biogas

production—Figure 6a), the economies of scale lower the aforementioned factors to 2.45 and 3.15 times for 2898 EUR·m^{-2} area specific SOFC cost and for SOFC areas escalating from 710 to 1540 m^2 (operation at 100% and 70% of the maximum power density, respectively); and to 2.95 and 4.24 times for 5269 EUR·m^{-2} area specific SOFC cost and the same SOFC area escalation.
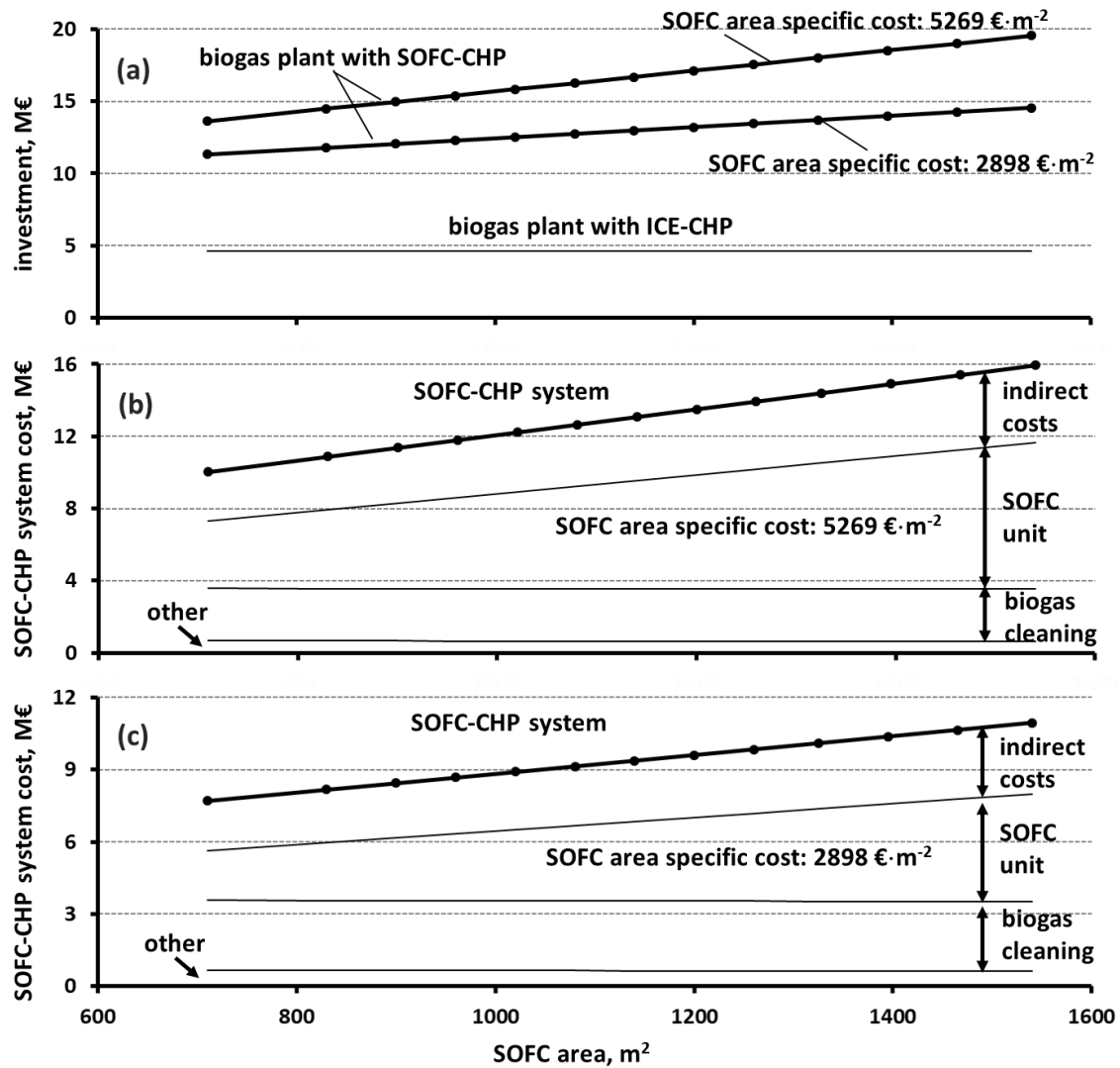

Figure 6. Initial investment of: (**a**) the conventional biogas-CHP plant with ICE-CHP, for 750 m^3·h^{-1} biogas production capacity, and of the corresponding SOFC-CHP system, for (**b**) 2898 EUR·m^{-2} SOFC area specific cost and (**c**) 5269 EUR·m^{-2} SOFC area specific cost.

Overall, the SOFC size escalation that increases the net power generation (P$_{NET}$) of the SOFC-CHP processes by 41.9%, regardless of the plant's size (from 0.64 to 0.90 MW for the small scale plant, and from 1.94 to 2.70 MW for the large scale one), results in a 23.4–37.2% increase in the small plant's investment cost and a 28.5–43.5% increase in the large plant's investment cost. Thus, the 14–62% increase in the SOFC-CHP net power generation, compared to the conventional ICE-CHP, is obtained by the increase in the initial investment by 2.80–3.45 and 3.24–4.45 times for the small scale plant, increasing with the SOFC's size and area specific cost, and by 2.45–3.15 and 2.95–4.24 times for the large scale plant, affected by the same factors.

The two main cost elements of the initial investment of the SOFC-CHP process (Figure 1) as well as of the total biogas-SOFC plant are the costs of the SOFC unit and of the biogas cleaning system, the second being independent of the employed SOFC unit

size since it aims to treat the total biogas production, of the plant. These two cost factors combined correspond to the 62–69% of the total investment for the SOFC-CHP system of Figure 1 and to the 44–56% of the total investment for the biogas-SOFC plant, depending upon the size of the employed SOFC unit for each plant capacity, as well as upon the plant's capacity (Figures 5 and 6). Solely, the SOFC unit investment cost corresponds to 20–51% of the investment for the CHP system of Figure 1 and to 14–42% of the total investment of the biogas plant, increasing with the size of the employed SOFC unit for each plant capacity, and with the capacity of the integrated biogas-CHP plant due to the non-linear escalation of the costs of the rest of the units of the integrated process.

Overall, the SOFC-CHP system cost was calculated to correspond to 68.2–75.2% of the total investment of the biogas-SOFC integrated plant, for 2898 EUR·m^{-2} SOFC's area specific cost, and the 73.6–82.6%, for 5269 EUR·m^{-2} SOFC's area specific cost, depending upon the integrated process capacity and the SOFC unit sizing. Thus, compared to the conventional biogas-CHP plant, for which the CHP-system cost corresponds to 22.0% of the total investment cost, the SOFC-CHP system corresponds to about or above three quarters of the total investment of biogas-CHP integrated plant.

The biogas-SOFC plant operation expenses were found to be 9.7–22.8% higher than the operation expenses of the conventional biogas plant due to the higher cost of the SOFC-CHP system and the maintenance and insurance expenses, which were regarded as proportional to this cost. Thus, for both the examined plant capacities, these expenses were affected by both the size of the employed SOFC and the assumed SOFC area specific cost, and ranged from 0.68 to 0.76 MEUR·a^{-1} for the 250 m^3·h^{-1} biogas production plant, and 1.93 to 2.15 MEUR·a^{-1} for the 750 m^3·h^{-1} biogas production plant. Biomass cost was constant for either the conventional or the biogas-SOFC plant (0.385 MEUR·a^{-1} for the 250 m^3·h^{-1} biogas capacity, and 1.155 MEUR·a^{-1} for the 750 m^3·h^{-1} biogas capacity), and corresponded to 50–56% of the annual operation expenses of the biogas-SOFC plant.

3.3. Feasibility Evaluation

The economic feasibility of the examined biogas-SOFC plants was assessed by the criteria of the Net Present Value (NPV), the Pay Back Time (PBT), based on NPV of the annual revenues, and the Internal Rate of Return (IRR). NPV is defined as:

$$\text{NPV} = \sum_0^n \frac{\text{EBTD}}{(1+r)^n} - I_T \quad [\text{EUR}] \tag{23}$$

where EBTD stands for the plant's annual Earnings Before Taxes and Depreciation, r is the annual discount rate, regarded herein at the typical value of 5.5%, n is the plant's lifetime (15 years) and I_T is the total initial investment. PBT is the time period for which the NPV value becomes zero, i.e., the time period at which the sum of the Net Present Value of the annual earnings becomes equal to the initial investment. On the other hand, IRR is defined as the annual discount rate that nullifies NPV:

$$\text{NPV} = 0 = \sum_0^n \frac{\text{EBTD}}{(1+\text{IRR})^n} - I_T \quad [\text{EUR}] \tag{24}$$

where IRR reflects the average annual return on the initial investment, i.e., the average depreciated annual profitability, divided by the investment. Thus, the IRR criterion, by its nature, pays more attention to the height of the initial investment, which is required in order for the annual revenues to be obtained, and tends to give a lower evaluation for investments of high initial cash outflow. On the other hand, NPV calculates the overall depreciated cash flows throughout the lifetime of an investment, counting the initial investment as just one of these cash flows. Thus, NPV gives a higher evaluation for investments of overall higher lifetime cash flows, and it is less affected by the initial cash outflow. The PBT, in turn, calculates the depreciated annual revenue cash flows up to the time that they become equal to the initial investment. Thus, PBT tends to devalue the effect of high annual

revenues since these high annual revenues are not accounted for in the total lifetime of the investment.

3.3.1. Economic Feasibility of the Small Scale Biogas-CHP Plant

Regarding the biogas plant of 250 m^3·h^{-1} biogas capacity, Figure 7 shows that the computed IRR values for the case of employing a SOFC-CHP system are considerably lower than the IRRs of the conventional case ICE-based biogas-CHP. The maximum calculated IRR, for the lower regarded SOFC area specific cost (2898 EUR·m^{-2}) was 13.4%, corresponding to almost one third of the IRR obtained for the conventional biogas ICE-CHP (34.4%). For the higher regarded SOFC area specific cost (5269 EUR·m^{-2}), this maximum IRR value further drops to 8.5%, i.e., to less than one quarter of the IRR of the ICE-CHP biogas plant.
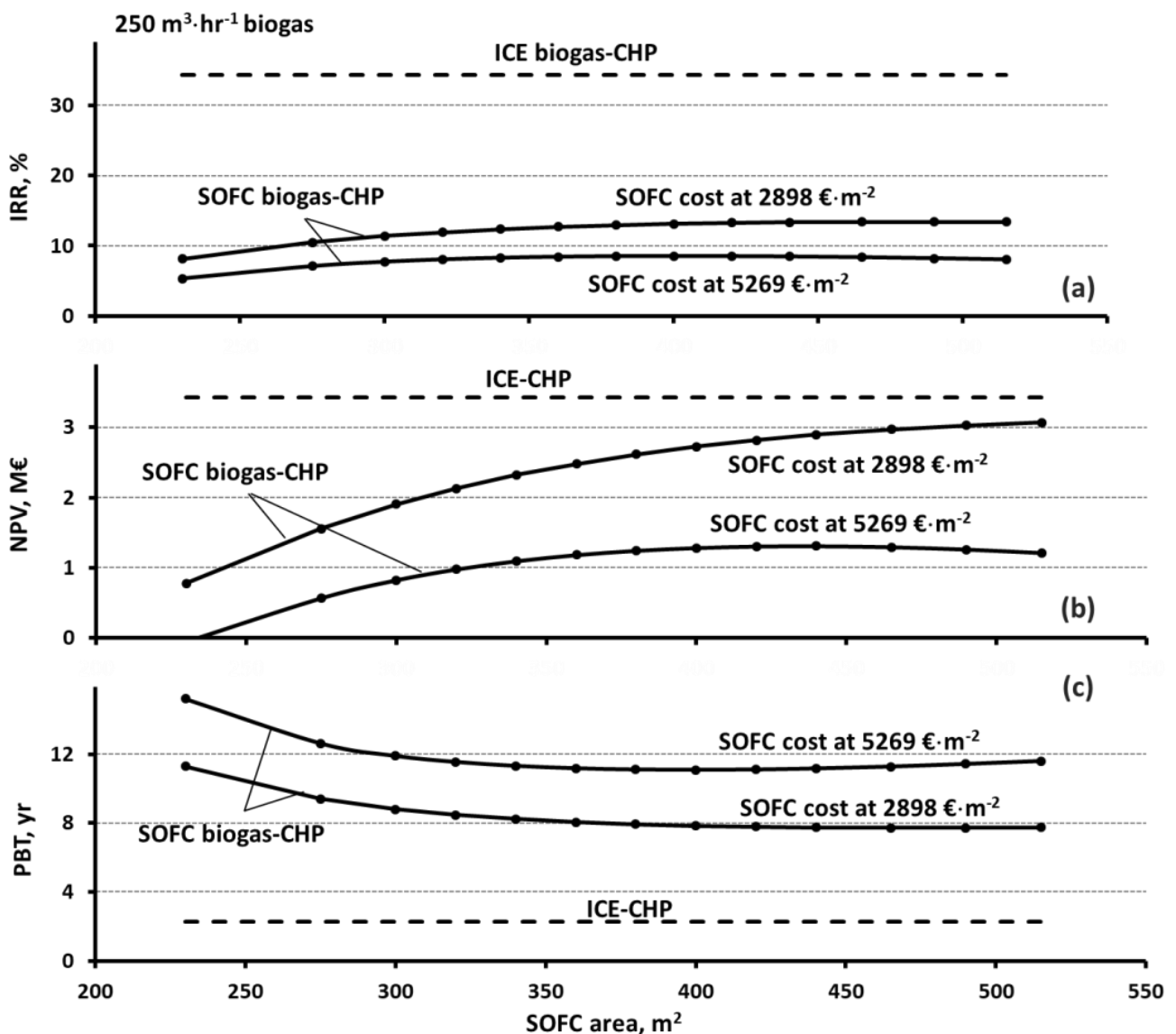

Figure 7. Dependence of: (**a**) IRR, (**b**) NPV and (**c**) PBT of the smaller scale biogas plant (250 m^3·h^{-1} biogas), on the size of the employed SOFC unit and its area specific cost, and their comparison to conventional biogas-CHP of the same biogas capacity.

Moreover, Figure 7a shows that for the lower regarded area specific cost of the SOFC, the IRR of the biogas-SOFC plant is maximized for SOFC area at 465 m^2, i.e., for a SOFC unit sized accordingly so as to operate at 75% of its maximum power density (MPD). On the other hand, for the higher area specific cost of the SOFC, the IRR is maximized for an

about 15% smaller SOFC unit of 400 m^2 surface area, i.e., for a SOFC unit sized to operate at 82.5% of its MPD. This observation denotes the effect of the SOFC cost on the optimum size of the employed SOFC unit.

Thus, in the case where the IRR criterion was chosen for the economic feasibility evaluation, the biogas-SOFC options were not found to be able to economically compete with the already established biogas-CHP with ICEs, even for the rather low SOFC technology costs, regarded herein. That is because the IRR criterion emphasizes the height of the initial investment that is required for the increased annual revenues of the biogas-SOFC plant. Thus, despite the up to 57% increase in the net generated power, the more than quadrupled initial investment considerably suppressed the IRR values of the SOFC-CHP biogas plant. Moreover, the increase in the size of the employed SOFC unit did not seem to drastically affect IRR, denoting that the increase in power generation for larger SOFC units is mostly counterbalanced by the increase in their cost. Nevertheless, IRR variates with the employed SOFC size, and according to the IRR criterion, the economic performance of the biogas-SOFC options are optimized for the employed SOFCs, which operate at 75–82.5% of the SOFC's MPD, depending upon the SOFC's area specific cost.

On the other hand, the NPV criterion (Figure 7b) shows that for the lower SOFC's specific cost (2898 EUR·m^{-2} or 1100 EUR·kW$_{el}$$^{-1}$, foreseen at 2035), the biogas-SOFC plant can obtain NPV values comparable to those of the conventional biogas-CHP, suggesting that the alteration IN the economic feasibility criterion alters the results of the feasibility assessment itself. Thus, the IRR criterion of Figure 7a renders the SOFC-CHP economic performance to fall considerably short compared to conventional biogas ICE-CHP, whereas, for the lower regarded SOFC cost, the NPV criterion attains a maximum value of EUR 3.07 M, which was comparable to the NPV of the conventional ICE-CHP (EUR 3.42 M). This was due to the fact that the NPV feasibility criterion evaluates the lifetime cash flow of an investment, suppressing the effect of the height of the required initial investment. Nonetheless, for the higher SOFC's specific cost (5269 EUR·m^{-2} or 2000 EUR·kW$_{el}$$^{-1}$, foreseen at 2030), the NPV dropped significantly, and its maximum calculated value was EUR 1.31 M, i.e., less than half the NPV of the conventional ICE-CHP.

For the low SOFC cost of 2898 EUR·m^{-2}, the maximum NPV of EUR 3.07 M was obtained for a SOFC unit sized to operate at 70% of its MPD, i.e., for a larger, compared to IRR, SOFC unit of 500 m^2 surface area. This fact denotes the effect of the feasibility criterion on the economically optimum size of the employed SOFC unit. Due to the nature of the NPV feasibility criterion, the NPV values are maximized for larger SOFC units, which along with the maximization of the initial investment, also maximize the overall revenues throughout the investment's lifetime. As expected, compared to IRR, the NPV criterion, which pays less attention to the initial investment in favor of the increased annual revenues, optimizes the biogas-SOFC CHP for larger and more expensive SOFC units, which obtain higher power generations and higher annual revenues. Nevertheless, for the higher SOFC's specific cost of 5269 EUR·m^{-2}, the optimum SOFC size was reduced to 440 m^2 (operation at 77.5% MPD) since the effect of the SOFC cost still causes the optimum size to be reduced to smaller and less expensive SOFC units. That is because the optimum SOFC size and operation point is calculated by the balance between the increased power generation and the increased cost of larger cells. Consequently, the more expensive the SOFC unit, the smaller the SOFC size that optimizes the economic performance of the biogas-SOFC plant.

The PBT criterion, in turn, reduces the positive effect of the SOFC-CHP's increased annual revenues by suppressing the time period for which it calculates these revenues, and magnifying the negative effect of the also increased initial investment. Thus, for the same initial investment, the NPV criterion calculates the increased revenues for the whole of the investment's lifetime, whereas the PBT calculates them for the shorter time period required for these revenues to become cumulatively equal to the initial investment. Consequently, the calculated PBTs (11.08–15.20 yr for 2.898 EUR·m^{-2} area specific SOFC cost and 7.72–11.29 yr for 5269 EUR·m^{-2} area specific SOFC cost) for the small scale biogas-SOFC plant (Figure 7c) are considerably higher than the Pay Back Time (3.08 yr) of the conventional biogas-ICE

CHP. For the economically optimum case of the low SOFC area specific cost and the optimized size of the employed SOFC unit, the minimum calculated PBT (7.72 yr) was considerably higher than the conventional plant's PBT; and the overall PBT-based economic evaluation was similar to that of the IRR criterion, rendering biogas-SOFC CHP plants as not able to be economically competitive with the conventional biogas-ICE CHP plants. Moreover, the economically optimum SOFC size, according to the PBT feasibility criterion, coincides with that calculated for the IRR criterion (465 m² SOFC, for the SOFC's specific cost at 1100 EUR·kW⁻¹, and 400 m² for the SOFC's specific cost 2000 EUR·kW⁻¹), giving a higher validation of the importance of the increased SOFC-CHP initial investment, over the effect of the increased annual revenues for larger and more expensive SOFC units.

In this context, Table 8 summarizes the main operational and economic features of the small biogas-CHP plants, as well as their feasibility performance indicators of IRR, NPV and PBT. Notably, the annual operation expenses of the biogas-SOFC plants are only slightly increased, compared to the conventional ones, despite the multiple times increase in the initial investment, and the consequent increase in the maintenance and insurance costs. This is due to the high share of the annual biomass cost, which is the same for both CHP options. It should also be mentioned that, despite the considerable net heat generation, especially for the conventional biogas plant, or for small employed SOFCs, that operate at MPD, the heat-related annual revenues are rather small compared to the electricity annual revenues due to the considerably lower heat shelling price (40 EUR·MWH$_{th}$⁻¹, compared to the 220 EUR·MWH$_{el}$⁻¹). Thus, the annual heat revenues correspond to 15% of the total annual revenues for the conventional biogas plant, dropping to 8% for the biogas-SOFC plant operating at MPD and to 1.5% for the biogas-SOFC operating at 70% of the MPD.

Table 8. Summary of the main operational and economic characteristics, and the feasibility performance of the smaller scale biogas-CHP plant.

Biogas Capacity, m³·h⁻¹		250.00			
	ICE		SOFC		
Operation point		MPD		70% MPD	
SOFC size, m²		230		515	
n_{el}, %	40	45.21		62.99	
Net elec. power, MW$_{el}$	0.558	0.635		0.901	
Net thermal power, MW$_{th}$	0.504	0.327		0.061	
SOFC spec. cost, EUR·kW⁻¹		1100	2000	1100	2000
SOFC spec. cost, EUR·m⁻²		2897.91	5268.93	2897.91	5268.93
Investment, EUR M	1.68	4.70	5.45	5.80	7.47
Operation exp. [1], MEUR·a⁻¹	0.62	0.68	0.69	0.74	0.76
IRR [2], %	34.36	8.13	5.33	13.38	8.04
NPV [3], EUR M	3.420	0.775	−0.055	3.070	1.212
PBT [4], yr	3.08	11.29	15.20	7.73	11.59

[1] Biomass cost 0.385 MEUR·yr⁻¹. [2] In total, 13.41% maximum, at 465 m² SOFC area (operating at 75% of the MPD), for SOFC specific cost 1100 EUR·kW⁻¹, and 8.52% maximum at 400 m² SOFC area (operating at 82.5% MPD), for SOFC specific cost 2000 EUR·kW⁻¹. [3] In total, EUR 3.070 M maximum at 515 m² SOFC area (operating at 70% of the MPD), for SOFC specific cost 1100 EUR·kW⁻¹, and EUR 1.308 M maximum at 440 m² SOFC area (77.5% MPD), for SOFC specific cost 2000 EUR·kW⁻¹. [4] A 7.72 yr minimum at 465 m² SOFC area (operating at 75% of the MPD), for SOFC specific cost 1100 EUR·kW⁻¹, and 11.08 yr minimum at 400 m² SOFC area (82.5% MPD), for SOFC specific cost 2000 EUR·kW⁻¹.

3.3.2. Economic Feasibility of the Large Scale Biogas-CHP Plant

The effect of the feasibility assessment criterion on the feasibility assessment itself becomes more profound for the case of the larger biogas plant of 750 m³·h⁻¹ biogas capacity. For this plant capacity, the IRR values of the SOFC-CHP biogas plant (Figure 8a) remain lower than the IRR of the conventional ICE-CHP biogas plant, and the PBT values are, accordingly, higher, both suggesting a deteriorating economic performance of the biogas-SOFC CHP. Conversely, the NPV values of the SOFC-based plant (Figure 7b) become considerably higher than those of the ICE biogas plant, suggesting that in the case where

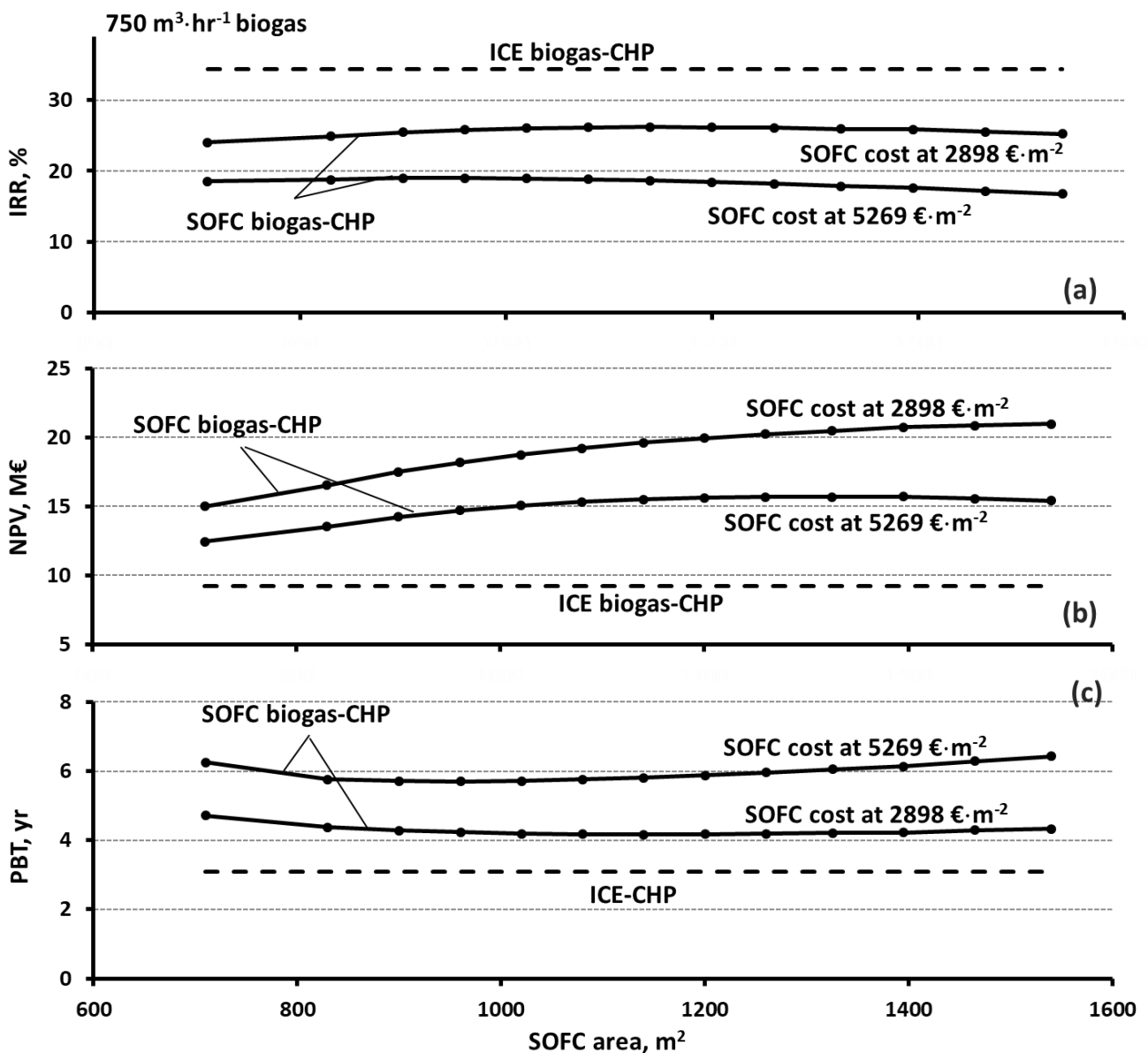the lifetime revenues are of prime interest, the economic performance of SOFC-CHP is considerably superior.

Figure 8. Dependence of: (**a**) IRR, (**b**) NPV and (**c**) PBT, of the smaller scale biogas plant (750 m^3·h^{-1} biogas), on the size of the employed SOFC unit and its area specific cost, and their comparison to conventional biogas-CHP of the same biogas capacity.

Regarding IRR, Figure 8a shows that, compared to the small plant capacity (Figure 7a), the IRR of the large plant increases significantly. For the lower assumed SOFC's area specific cost of 2.898 EUR·m^{-2} (foreseen at 2035), the maximum IRR value reaches 26.9%, rendering the large scale biogas-SOFC plant as economically feasible, although of lower economic effectiveness compared to the conventional biogas-ICE CHP (IRR: 34.4%). Nonetheless, for the higher regarded SOFC's area specific cost of 5269 EUR·m^{-2} (foreseen at 2030), the maximum IRR value drops to 19.0%, rendering the biogas-SOFC plants as having marginal economic feasibility, with comparatively lower economic performance. These significant IRR improvements with the plant's capacity denote the scale effect on the economic viability, and reflect the impact of the fact that the initial investment of the larger plant does not increase proportionally to its power output and its annual revenues. Thus, although the net

power generation, and consequently the annual revenues, of the large scale plant is 3 times higher than the net power generation and the annual revenues of the small scale plant, its initial investment is only 1.95–2.41 times higher, for the lower regarded SOFC area specific cost, depending upon the employed SOFC's size, and 2.50–2.62 times higher, for the higher regarded SOFC area specific cost, still depending upon the employed SOFC's size.

In the case where the NPV criterion is used for the investment validation, the biogas-SOFC options exhibit considerably improved feasibility prospects compared to the conventional biogas-ICE plant, of the same biogas capacity, even for the higher examined area specific SOFC cost. Regarding the lower SOFC's area specific cost, the calculated NPV was maximized at EUR 21.0 M, more than double the NPV (EUR 9.3 M) of the conventional ICE biogas-CHP. For the higher SOFC's specific cost, the NPV was maximized at EUR 15.7 M, i.e., about 50% higher than the NPV (EUR 9.3 M) of the conventional ICE biogas-CHP, and 25% lower than the maximum NPV for the lower SOFC area specific cost.

Notably, for the lower area specific cost of the SOFC, the NPV maximization is obtained for the maximum examined surface area (1540 m^2) and the maximum investment cost of the employed SOFC unit, which operates at higher efficiency and also maximizes power generation and annual revenues. This is due to the nature of the NPV criterion, which is mostly determined by the annual income cash flows, throughout the investment's lifetime, and is less affected by the height of the initial investment. Still, for the lower SOFC's area specific cost, the NPV drops to EUR 15.0 M, for the minimum SOFC surface area (710 m^2) of minimized investment cost. That is because the employment of a small SOFC unit decreases the efficiency (Figure 2), and consequently the power generation and the annual revenues, throughout the plant's lifetime, and despite the decrease in the employed SOFC cost. For the higher area specific cost of the SOFC, the NPV maximization is obtained for a smaller SOFC unit of 1325 m^2, reflecting the effect of the SOFC's area specific cost on the optimization of the employed SOFC's size. As for the case of the small biogas plant, the PBT economic criterion resulted in an economic assessment that coincided with that of the IRR criterion. Thus, the calculated PBTs of the SOFC-CHP options were higher than the PBT of the conventional biogas-ICE CHP, and the optimum SOFC size was shifted to smaller SOFC units of 960 and 1140 m^2, decreasing with the increase in area specific SOFC cost. The minimum calculated PBTs dropped from 5.7 to 4.17 yr, with the increase in the regarded area specific SOFC cost, compared to the 3.08 yr of the conventional ICE-CHP biogas plant, rendering the SOFC options economically viable but of lower economic performance.

In this context, Table 9 summarizes the main operational and economic features of the large scale biogas-CHP plants, as well as their feasibility performance indicators of IRR and NPV. Compared to the small biogas plants (Table 8), the overall economic performance of both the SOFC and ICE CHP options was calculated to be improved due to the fact that the increase in the initial investment, for the large scale plants, is lower than the increase in the power output. For both the examined plant scales, compared to a maximum of 40% electrical efficiency for the conventional diesel engine biogas-CHP, the SOFC-based CHP system, of 45.2–63.0% electrical efficiency, was computed to generate 13–57% more power, depending upon the employed SOFC size and denoting both the ability of SOFCs to drastically increase the power output of biogas-CHP plants, as well as the remarkable effect of the size of the employed SOFC unit on this power output. Nonetheless, this increase in electricity generation and annual revenues is obtained at the expense of much higher initial investment. For a SOFC power-specific cost at 2000 EUR·kWel^{-1}, foreseen by 2030, the total investment of the biogas-SOFC plant was calculated to be 3.15–4.45 times higher than the conventional ICE biogas plant, depending upon the process scale and the employed SOFC size. For SOFC specific cost at 1100 EUR·kWel^{-1}, foreseen by 2035, the total investment increase was calculated at 2.45–3.45 times, compared to the conventional biogas-CHP.

In cases where the IRR or the PBT criteria are chosen for the economic feasibility evaluation, the biogas-SOFC options were not found to be capable of economically competing with the already established biogas-CHP with ICEs, even for the rather low SOFC technology costs assumed herein. That is because these criteria emphasize the height

of the initial investment, which is required in order to achieve the efficiency and power generation gains. Thus, despite the up to 57% increase in the net generated power, the more than quadrupled initial investment suppressed the IRR values and substantially increased the PBTs of the biogas-SOFC CHP, compared to the conventional biogas-CHP options. Moreover, the increase in the size of the employed SOFC unit did not seem to remarkably affect either IRR or PBT, denoting that for these criteria, the increase in power generation for larger SOFC units, is mostly counterbalanced by the increase in their cost. Within these mild variations of IRR and PBT values, with the employed SOFC size, the economic performance of the biogas-SOFC options tends to be optimized for SOFCs that operate at 75–82.5% of the SOFC's MPD for the small scale plant and 85–92.5% MPD for the large scale plant.

Table 9. Summary of the main operational and economic characteristics, and the feasibility performance of the larger scale biogas-CHP plant.

Biogas Capacity, m³·h⁻¹		750.00			
	ICE	SOFC			
Operation point		MPD		70% MPD	
SOFC size, m²		710		1.540	
n_{el}, %	40	45.21		62.99	
Net elec. power, MW$_{el}$	1.674	1.944		2.701	
Net thermal power, MW$_{th}$	1.512	0.941		0.184	
SOFC spec. cost, €·kW⁻¹		1100	2000	1100	2000
SOFC spec. cost, €·m⁻²		2897.91	5268.93	2897.91	5268.93
Investment, M€	4.62	11.32	14.55	13.62	19.55
Operation exp. [1], M€·a⁻¹	1.75	1.93	1.95	2.10	2.15
IRR [2], %	34.41	24.05	18.51	25.25	16.75
NPV [3], M€	9.25	15.02	12.46	20.97	15.41
PBT [4], yr	2.27	4.72	6.25	4.33	6.43

[1] Biomass cost 1.155 MEUR·yr⁻¹. [2] In total, 26.19% maximum at 1140 m² SOFC area (operating at 85% of the MPD), for SOFC specific cost 1100 EUR·kW⁻¹, and 19.00% maximum at 960 m² SOFC area (92.5% of the MPD), for SOFC specific cost 2000 EUR·kW⁻¹. [3] In total, EUR 20.967 M maximum at 1540 m² SOFC area (operating at 70% of the MPD), for SOFC specific cost 1100 EUR·kW⁻¹, and EUR 15.712 M maximum at 1395 m² SOFC area (75% of the MPD), for SOFC specific cost 2000 EUR·kW⁻¹. [4] A 4.17 yr minimum at 1140 m² SOFC area (operating at 85% of the MPD), for SOFC specific cost 1100 EUR·kW⁻¹, and 5.70 yr minimum at 960 m² SOFC area (92.5% MPD), for SOFC specific cost 2000 EUR·kW⁻¹.

On the other hand, the use of the NPV criterion significantly alters the overall picture. Thus, for the low SOFC technology costs (1100 EUR·kWel⁻¹), even the smaller scale biogas-SOFC plant can economically compete with diesel engine biogas-CHP. For the same criterion, the larger scale biogas-SOFC plant was found to be considerably more economically effective than the corresponding conventional biogas-CHP, even for the higher SOFC technology costs (2000 EUR·kWel⁻¹) targeted for 2030. That was due to the fact that the NPV feasibility criterion evaluates the total cash flow of an investment, suppressing the effect of the height of the required initial investment. As expected, and still due to the nature of the NPV feasibility criterion, the NPV values tend to be maximized for larger SOFC units, which also maximize the initial investment. Thus, for a 1100 EUR·kWel⁻¹ specific SOFC cost and either the smaller or the larger plant capacity, the NPV is maximized for the larger employed SOFC that operates at 70% of the MPD, i.e., for the SOFC unit of maximum cost, which maximized the initial investment. That was because the larger employed SOFC also maximized the net power generation and consequently the annual revenues of the plant. For a 2000 EUR·kWel⁻¹ specific SOFC cost, the economically optimum size slightly shifts to smaller SOFC units that operate at about 75–77.5% of the MPD, to compromise for the increase in the initial investment for larger cells, with the lower net power generation and annual revenues for smaller ones.

Overall, in the case where the lifetime cash flow of the investment, regardless of the height of the investment itself, is of the investors' prime interest, and the NPV feasibility criterion is chosen for the economic assessment, then the biogas-SOFC technology was found to be economically superior (under the regarded cost and bio-electricity pricing assumptions) compared to the conventional one, despite the up to more than 4 times

higher initial investment. That is because of its increased electricity generation and annual profitability, which stands for both of the assumed area specific costs of the employed SOFC. Nonetheless, this much higher required investment for the SOFC-biogas plants suppressed their IRR and PBT values, despite their overall much higher electricity revenues and profitability. Regarding the effect of the size of the employed SOFC unit, the IRR and the PBT criteria were maximized for smaller SOFC sizes, compared to the economically optimum SOFC sizes for NPV maximization.

These findings can be affected by several parameters. Thus, for lower bio-electricity prices than the 220 EUR·MWh^{-1} regarded herein, the biogas-SOFC advantage of having substantially increased annual incomes would be weakened, thus deteriorating their NPV-assessed performance. On the other hand, a potentially higher biomass cost than the 40 EUR·tn^{-1} regarded herein would represent a proportionally higher reduction in the biogas-ICE annual revenues, thus suppressing their NPV performance and favouring the assessment of the biogas-SOFC option. The same also stands for the regarded plant's lifetime. Increasing the plant's lifetime to 20 years, which is often regarded in the literature [44,45,65], would disproportionally improve the biogas-SOFC NPV performance compared to that of the conventional biogas-ICE due to its drastically increased net power generation and annual revenues. Thus, for increased plant lifetimes, the biogas-SOFC options would appear to be economically superior for higher SOFC costs, and probably sooner than 2030. Finally, potentially reduced costs of biogas cleaning costs, compared to the ones regarded herein, are expected to improve both the IRR and the NPV performance of the biogas-SOFC options by reducing the overall initial investment. Nonetheless, the performed analysis clearly demonstrated that the sizing of the employed SOFC unit, can majorly affect the economic performance of biogas-SOFC plants, whereas the choice of the economic feasibility criterion can drastically alter the assessment of this performance. Moreover, the optimum SOFC size for biogas-SOFC CHP-plants depends not only upon the SOFC technology cost but also on the choice of the feasibility criterion.

4. Conclusions

In the present work, a biogas-SOFC CHP process was thermodynamically simulated in order to correlate its main operational features with its overall performance and investment cost. Incorporating this process as the CHP system of a biogas plant within the BPCT tool of a biogas plant's economic evaluation, the present work estimated the economic feasibility of biogas-SOFC plants and its comparison with the economic feasibility of the already widespread biogas-CHP plants with ICE-CHPs.

Against the already widespread biogas-CHP with ICE, the SOFC-based biogas-CHP was calculated to obtain remarkably higher efficiency and overall power generation, but at the expense of a much higher initial investment, whereas both the power generation and the initial investment increased with the size of the employed SOFC unit. The present work examined the balance between the increased investment costs and the increased power generation of biogas-SOFC plants, in terms of their overall economic performance and in comparison with the economic performance of the conventional biogas-CHP with ICE. Among several parameters that affect this balance, the present work has focused on the sizing of the employed SOFC unit, as well as on the feasibility criteria utilized for the economic assessment, based upon realistic assumptions regarding the most crucial cost factors of biogas generation and the employed CHP systems, the cost of biomass, the electricity/heat pricing and the foreseen SOFC costs.

The main conclusion was that as the SOFC technology costs approach the targeted values for 2030 and 2035, the biogas-SOFC CHP option approaches economic competitiveness against the widespread current option of ICE-based biogas CHP. This competitiveness is strongly depended upon the choice of the feasibility criterion as well as upon the choice of the economically optimum size of the employed SOFC unit. Moreover, the choice of the economically optimum SOFC unit also depends upon the choice of the assessment criterion. In the case where the overall lifetime cash flow and not the return on the investment is of

prime interest, then the NPV criterion assesses the biogas-SOFC option as economically superior to the established biogas-ICE one, even for SOFC technology costs higher than the ones targeted for 2030.

Appendix A. Thermodynamic Calculations

For the calculation of sensible heat in the currents of the process of Figure 1, the calculation of the extent and the thermal effect of the involved reactions, and of the power produced or consumed, in the system components and processes of the same figure, the analytical expressions of the specific heat capacity were used at constant pressure (cp):

$$c_P^i = \frac{\left(a + b \times T + c \times T^2 + d \times T^3\right)}{1000} \quad [kJ\cdot kmol^{-1}\cdot K^{-1}] \tag{A1}$$

where i indicates the chemical compound or element (CH_4, CO_2, H_2O, N_2, H_2S, NH_3, O_2, H_2, CO, Ar, SO_2), T is the absolute temperature [K] and a, b, c κα ι d are the relative constants, which are given in Table A1 [66].

Table A1. Thermodynamic values [66].

	C_P, kJ·kmol^{-1}·K^{-1}				Δh^o	Δs^o	Δg^o
	a	b	c	d	kJ·kmol^{-1}	kJ·kmol^{-1}·K^{-1}	kJ·kmol^{-1}
CH_4	19.890	5.02×10^{-2}	1.27×10^{-5}	-1.10×10^{-8}	$-74,520$	-80.94	$-50,400$
CO_2	22.260	5.98×10^{-2}	-3.50×10^{-5}	7.47×10^{-9}	$-393,514$	2.92	$-394,384$
$H_2O_{(g)}$	32.240	1.92×10^{-3}	1.06×10^{-5}	-3.60×10^{-9}	$-241,826$	-44.41	$-228,592$
N_2	28.990	-1.57×10^{-3}	8.08×10^{-6}	-2.87×10^{-9}			
H_2S	34.200				$-20,100$		
NH_3	27.568	2.56×10^{-2}	9.91×10^{-6}	-6.69×10^{-9}	$-46,200$		
O_2	25.480	1.52×10^{-2}	-7.16×10^{-6}	1.31×10^{-9}			
H_2	29.110	-1.92×10^{-3}	4.00×10^{-6}	-8.70×10^{-10}			
CO	28.160	1.68×10^{-3}	5.37×10^{-6}	-2.22×10^{-9}	$-110,525$	89.75	$-137,269$
Ar	20.785						
SO_2	25.780	5.80×10^{-2}	-3.81×10^{-5}	8.61×10^{-9}	$-296,100$		

In the same table, values of the standard enthalpy of formation (Δh^o) and standard entropy of formation (Δs^o) of the involved chemical compounds (standard conditions: $T^o = 298.15$ K and $P^o = 101,325$ kPa) are given. Gibbs free energy is defined as:

$$\Delta g^o = \Delta h^o - T^o \times \Delta s^o \quad [kJ\cdot kmol^{-1}] \tag{A2}$$

Sensible heat Q_J in stream J of the process was calculated by Equation:

$$Q_J = \sum_i f_i \times q_i \quad [kJ\cdot s^{-1}] \tag{A3}$$

where f_i is the molar flow of component i at stream J ($kmol \cdot s^{-1}$) and q_i is the molar sensible heat ($kmol \cdot s^{-1}$) of component i at temperature T_J of the stream J, which is calculated by the integral:

$$q_i = \int_{T_{ref}}^{T_J} c_P^i dT \quad [kJ \cdot kmol^{-1}] \tag{A4}$$

where T_{ref} is the reference temperature, which for the present study was considered equal to 25 °C (298.15 K—the temperature at which the sensible heat of any substance is set to zero).

The change in the molecular entropy ($kJ \cdot kmol^{-1} \cdot K^{-1}$) of component I from the standard conditions to the conditions of the stream J, was calculated by the integral equation:

$$\Delta s_i = \int_{T_{ref}}^{T_J} \frac{c_P^i}{T} dT \quad [kJ \cdot kmol^{-1}] \tag{A5}$$

which was used both for the calculation of the isentropic work in the compression and expansion devices of the process, and for the calculation of the equilibrium position of the chemical reactions when this was deemed necessary. The change in the free energy of the reactions (ΔG_{rxn}), bounded by the equilibrium, was calculated from the equation:

$$\Delta G_{rxn} = \sum_p A_P \times \Delta g_P - \sum_r A_r \times \Delta g_r \quad [kJ \cdot kmol^{-1}] \tag{A6}$$

where r and p denote the reactants and the products of the reaction, A is the corresponding stoichiometric coefficient and Δg_i is the molar free energy of the component i at the temperature T of the reaction, which is calculated from the equation:

$$\Delta g_i^T = \Delta h_i^T - T \times \Delta s_i^T \quad [kJ \cdot kmol^{-1}] \tag{A7}$$

where Δh_i^T is the molar enthalpy of component i at the reaction temperature T, calculated from the equation:

$$\Delta h_i^T = \Delta h_i^o + \int_{T_{ref}}^{T} c_P^i dT \quad [kJ \cdot kmol^{-1}] \tag{A8}$$

and Δs_i^T is the molar entropy of component i at the temperature T of the reaction, calculated from the equation:

$$\Delta s_i^T = \Delta s_i^o + \int_{T_{ref}}^{T} \frac{c_P^i}{T} dT \quad [kJ \cdot kmol^{-1}] \tag{A9}$$

The pressure ratio, in the equations for calculating entropy changes, has been omitted, due to negligible pressure changes, throughout the process and the system components.

References

1. Bremond, U.; Bertrandias, A.; Steyer, J.; Bernet, N. A vision of European biogas sector development towards 2030: Trends and challenges. *J. Clean. Prod.* **2021**, *287*, 125065. [CrossRef]
2. Gustafsson, M.; Anderberg, S.; Gustafsson, M.; Anderberg, S. Biogas policies and production development in Europe: A comparative analysis of eight countries Biogas policies and production development in Europe: A comparative analysis of eight countries. *Biofuels* **2022**, *13*, 931–944. [CrossRef]
3. Kampman, B.; Leguijt, C.; Scholten, T.; Tallat-Kelpsaite, J.; Brückmann, R.; Maroulis, G.; Lesschen, J.P.; Meesters, K.; Sikirica, N.; Elbersen, B. *Optimal Use of Biogas from WASTE Streams: An Assessment of the Potential of Biogas from Digestion in the EU beyond 2020*; Directorate-General for Energy, European Commission: Brussels, Belgium, 2016.
4. Mertins, A.; Wawer, T. How to use biogas? A systematic review of biogas utilization pathways and business models. *Bioresour. Bioprocess.* **2022**, *9*, 59. [CrossRef]
5. Saadabadi, S.A.; Thallam, A.; Fan, L.; Lindeboom, R.E.F.; Spanjers, H.; Aravind, P.V. Solid Oxide Fuel Cells fuelled with biogas: Potential and constraints. *Renew. Energy* **2019**, *134*, 194–214. [CrossRef]
6. Lantz, M. The economic performance of combined heat and power from biogas produced from manure in Sweden—A comparison of different CHP technologies. *Appl. Energy* **2012**, *98*, 502–511. [CrossRef]

7. Lanzini, A.; Madi, H.; Chiodo, V.; Papurello, D.; Maisano, S.; Santarelli, M.; Van Herle, J. Dealing with fuel contaminants in biogas-fed solid oxide fuel cell (SOFC) and molten carbonate fuel cell (MCFC) plants: Degradation of catalytic and electro-catalytic active surfaces and related gas purification methods. In *Progress in Energy and Combustion Science*; Elsevier Ltd.: Amsterdam, The Netherlands, 2017; Volume 61, pp. 150–188. [CrossRef]
8. Yingjian, L.; Qi, Q.; Xianghu, H.; Jiezhi, L. Energy balance and efficiency analysis for power generation in internal combustion engine sets using biogas. *Sustain. Energy Technol. Assess.* **2014**, *6*, 25–33. [CrossRef]
9. Van Herle, J.; Maréchal, F.; Leuzenberger, S.; Membrez, Y.; Bucheli, O.; Favrat, D. Process flow model of solid oxide fuel cell system supplied with sewage biogas. *J. Power Sources* **2004**, *131*, 127–141. [CrossRef]
10. Wongchanapai, S.; Iwai, H.; Saito, M.; Yoshida, H. Performance evaluation of a direct-biogas solid oxide fuel cell-micro gas turbine (SOFC-MGT) hybrid combined heat and power (CHP) system. *J. Power Sources* **2013**, *223*, 9–17. [CrossRef]
11. Cigolotti, V.; Matteo Genovese, M.; Fragiacomo, P. Comprehensive Review on Fuel Cell Technology for Stationary Applications as Sustainable and Efficient Poly-Generation Energy Systems. *Energies* **2021**, *14*, 4963. [CrossRef]
12. Hagen, A.; Langnickel, H.; Sun, X. Operation of solid oxide fuel cells with alternative hydrogen carriers. *Int. J. Hydrog. Energy* **2019**, *44*, 18382–18392. [CrossRef]
13. Cigolotti, V.; Massi, E.; Moreno, A.; Polettini, A.; Reale, F. Biofuels as opportunity for MCFC niche market application. *Int. J. Hydrog. Energy* **2008**, *33*, 2999–3003. [CrossRef]
14. Ciccoli, R.; Cigolotti, V.; Lo Presti, R.; Massi, E.; Mcphail, S.J.; Monteleone, G.; Moreno, A.; Naticchioni, V.; Paoletti, C.; Simonetti, E.; et al. Molten carbonate fuel cells fed with biogas: Combating H2S. *Waste Manag.* **2010**, *30*, 1018–1024. [CrossRef]
15. Mc Phail, S.J.; Aarva, A.; Devianto, H.; Bove, R.; Moreno, A. SOFC and MCFC: Commonalities and opportunities for integrated research. *Int. J. Hydrog. Energy* **2010**, *36*, 10337–10345. [CrossRef]
16. Hydrogen Europe. *Strategic Research and Innovation Agenda Final Draft*; Hydrogen Europe: Brussels, Belgium, 2020.
17. Wasajja, H.; Lindeboom, R.E.F.; Van Lier, J.B.; Aravind, P.V. Techno-economic review of biogas cleaning technologies for small scale off- grid solid oxide fuel cell applications. *Fuel Process. Technol.* **2020**, *197*, 106215. [CrossRef]
18. Abanades, S.; Abbaspour, H.; Ahmadi, A.; Das, B.; Ehyael, M.; Esmaeilion, F.; El Haj Assad, M.; Hajilounezhad, T.; Jamali, D.; Hmida, A.; et al. A critical review of biogas production and usage with legislations framework across the globe Ministry of Finance. *Int. J. Environ. Sci. Technol.* **2022**, *19*, 3377–3400. [CrossRef]
19. Staniforth, J.; Kendall, K. Biogas powering a small tubular solid oxide fuel cell. *J. Power Sources* **1998**, *71*, 275–277. [CrossRef]
20. Van Herle, J.; Marechal, F.; Leuenberger, S.; Favrat, D. Energy balance model of a SOFC cogenerator operated with biogas. *J. Power Sources* **2003**, *118*, 375–383. [CrossRef]
21. Van Herle, J.; Membrez, Y.; Bucheli, O. Biogas as a fuel source for SOFC co-generators. *J. Power Sources* **2004**, *127*, 300–312. [CrossRef]
22. Girona, K.; Laurencin, J.; Petitjean, M.; Fouletier, J.; Lefebvre-Joud, F. SOFC running on biogas: Identification and experimental validation of "Safe" operating conditions. *ECS Trans.* **2009**, *25*, 1041–1050. [CrossRef]
23. Murphy, D.; Richards, A.; Colclasure, A.; Rosensteel, W.; Sullivan, N. Biogas Fuel Reforming for Solid Oxide Fuel Cells. *ECS Trans.* **2011**, *35*, 2653–2667. [CrossRef]
24. Xu, C.; Zondlo, J.; Gong, M.; Elizalde-Blancas, F.; Liu, X.; Celik, I. Tolerance tests of H2S-laden biogas fuel on solid oxide fuel cells. *J. Power Sources* **2010**, *195*, 4583–4592. [CrossRef]
25. Shiratori, Y.; Oshima, T.; Sasaki, K. Feasibility of direct-biogas SOFC. *Int. J. Hydrog. Energy* **2008**, *33*, 6316–6321. [CrossRef]
26. Laycock, C.; Staniforth, J.; Ormerod, M. Improving the Sulphur Tolerance of Nickel Catalysts for Running Solid Oxide Fuel Cells on Waste Biogas. *ECS Trans.* **2009**, *16*, 177. [CrossRef]
27. Jahn, M.; Michaelis, A.; Näke, R.; Weder, A.; Heddrich, M. Simple and robust biogas-fed SOFC system with 50% electric efficiency—Modelling and Experimental results. In Proceedings of the 10th European SOFC Forum, Lucerne, Switzerland, 26–29 June 2012.
28. Hagen, A.A.; Winiwarter, A.; Langnickel, H.; Johnson, G. SOFC operation with real biogas. *Fuel Cell.* **2017**, *17*, 854–861. [CrossRef]
29. Papurello, D.; Borchiellini, R.; Bareschino, P.; Chiodo, V.; Freni, S.; Lanzini, A.; Pepe, F.; Ortigoza, G.; Santarelli, M. Performance of a solid oxide fuel cell short-stack with biogas feeding. *Appl. Energy* **2014**, *125*, 254–263. [CrossRef]
30. Piroonlerkgul, P.; Assabumrungrat, S.; Laosiripojana, N.; Adesina, A.A. Selection of appropriate fuel processor for biogas-fuelled SOFC system. *Chem. Eng. J.* **2008**, *140*, 341–351. [CrossRef]
31. Shiratori, Y.; Ijichi, T.; Oshima, T.; Sasaki, K. Internal reforming SOFC running on biogas. *Int. J. Hydrog. Energy* **2010**, *35*, 7905–7912. [CrossRef]
32. Tjaden, B.; Gandiglio, M.; Lanzini, A.; Santarelli, M.; Jarvinen, M. Small-scale biogas-SOFC plant: Technical analysis and assessment of different fuel reforming options. *Energy Fuels* **2014**, *28*, 4216–4232. [CrossRef]
33. Farhad, S.; Yoo, Y.; Hamdullahpur, F. Effects of fuel processing methods on industrial scale biogas-fuelled solid oxide fuel cell system for operating in wastewater treatment plants. *J. Power Sources* **2010**, *195*, 1446–1453. [CrossRef]
34. De Arespacochaga, N.; Valderrama, C.; Peregrina, C.; Mesa, C.; Bouchy, L.; Cortina, J.L. Evaluation of a pilot-scale sewage biogas powered 2.8 kWe Solid Oxide Fuel Cell: Assessment of heat-to-power ratio and influence of oxygen content. *J. Power Sources* **2015**, *300*, 325–335. [CrossRef]

35. Gandiglio, M.; Lanzini, A.; Santarelli, M.; Pierluigi Leone, P. Design and Balance-of-Plant of a Demonstration Plant with a Solid Oxide Fuel Cell Fed by Biogas from Waste-Water and Exhaust Carbon Recycling for Algae Growth. *J. Fuel Cell Sci. Technol.* **2014**, *11*, 031003–031016. [CrossRef]

36. Gandiglio, M.; Lanzini, A.; Santarelli, M.; Acri, M.; Hakala, T.; Rautanen, M. Results from an industrial size biogas-fed SOFC plant (the DEMOSOFC project). *Int. J. Hydrog. Energy* **2019**, *45*, 5449–5464. [CrossRef]

37. Aravind, P.V.; Cavalli, A.; Patel, H.C.; Recalde, M.; Saadabadi, A.; Tabish, A.N.; Botta, G.; Thallam Tattai, A.; Teodoru, A.; Hajimolana, Y.; et al. Opportunities and Challenges in Using SOFCs in Waste to Energy Systems. *ECS Trans.* **2017**, *78*, 209–218. [CrossRef]

38. Langnickel, H.; Rautanen, M.; Gandiglio, M.; Santarelli, M.; Hakala, T.; Acri, M.; Kiviaho, J. Efficiency analysis of 50 kWe SOFC systems fueled with biogas from waste water. *J. Power Sources Adv.* **2020**, *2*, 100009. [CrossRef]

39. Santarelli, M.; Gandiglio, M.; Acri, M.; Hakala, T.; Rautanen, M.; Hawkes, A. Results from industrial size biogas-fed SOFC plant (DEMOSOFC project). *Ecs Trans.* **2019**, *91*, 107–116. [CrossRef]

40. Gandiglio, M.; Drago, D.; Santarelli, M. Techno-economic Analysis of a Solid Oxide Fuel Cell Installation in a Biogas Plant Fed by Agricultural Residues and Comparison with Alternative Biogas Exploitation Paths. *Energy Procedia* **2016**, *101*, 1002–1009. [CrossRef]

41. Baldinelli, A.; Barelli, L.; Bidini, G. On the feasibility of on-farm biogas-to-electricity conversion: To what extent is solid oxide fuel cells durability a threat to break even the initial investment? *Int. J. Hydrog. Energy* **2018**, *43*, 16971–16985. [CrossRef]

42. Papadias, D.D.; Ahmed, S.; Kumar, R. Fuel quality issues with biogas energy: An economic analysis for a stationary fuel cell system. *Energy* **2012**, *44*, 257–277. [CrossRef]

43. Trendewicz, A.A.; Braun, R.J. Techno-economic analysis of solid oxide fuel cell-based combined heat and power systems for biogas utilization at wastewater treatment facilities. *J. Power Sources* **2013**, *233*, 380–393. [CrossRef]

44. Sechi, S.; Giarola, S.; Lanzini, A.; Gandiglio, M.; Santarelli, M.; Oluleye, G.; Hawkes, A. A bottom-up appraisal of the technically installable capacity of biogas-based solid oxide fuel cells for self-power generation in wastewater treatment plants. *J. Environ. Manag.* **2021**, *279*, 111753. [CrossRef]

45. Oluleye, G.; Gandiglio, M.; Santarelli, M.; Hawkes, A. Pathways to commercialisation of biogas fuelled solid oxide fuel cells in European wastewater treatment plants. *Appl. Energy* **2021**, *282*, 116127. [CrossRef]

46. Economic Calculation Tool for Biogas Plants. Available online: https://www.big-east.eu/downloads/downloads.html (accessed on 24 June 2022).

47. Alves, H.; Bley, C., Jr.; Niklevicz, R.; Frigo, E.; Frigo, M.; Coimbra-Araújo, C. Overview of hydrogen production technologies from biogas and the applications in fuel cells. *Int. J. Hydrog. Energy* **2013**, *38*, 5215–5225. [CrossRef]

48. Bocci, E.; Di Carlo, A.; McPhail, S.J.; Gallucci, K.; Foscolo, P.U.; Moneti, M.; Villarini, M.; Carlini, M. Biomass to fuel cells state of the art: A review of the most innovative technology solutions. *Int. J. Hydrog. Energy* **2014**, *39*, 21876–21895. [CrossRef]

49. Abatzoglou, N.; Boivin, S. A review of biogas purification processes. *Biofuels Bioprod. Biorefining* **2009**, *3*, 42–71. [CrossRef]

50. Lanzini, A.; Leone, P. Experimental investigation of direct internal reforming of biogas in solid oxide fuel cells. *Int. J. Hydrog. Energy* **2010**, *35*, 2463–2476. [CrossRef]

51. Lin, Y.; Zhan, Z.; Liu, J.; Barnett, S.A. Direct operation of solid oxide fuel cells with methane fuel. *Solid State Ion.* **2005**, *176*, 1827–1835. [CrossRef]

52. Klein, J.M.; Hénault, M.; Roux, C.; Bultel, Y.; Georges, S. Direct methane solid oxide fuel cell working by gradual internal steam reforming: Analysis of operation. *J. Power Sources* **2009**, *193*, 331–337. [CrossRef]

53. Lanzini, A.; Kreutz, T.G.; Martelli, E.; Santarelli, M. Energy and economic performance of novel integrated gasifier fuel cell (IGFC) cycles with carbon capture. *Int. J. Greenh. Gas Control* **2014**, *26*, 169–184. [CrossRef]

54. Borello, D.; Evangelisti, S.; Tortora, E. Modelling of a CHP SOFC system fed with biogas from anaerobic digestion of municipal waste integrated with solar collectors and storage unit. *Int. J. Thermodyn.* **2013**, *16*, 28–35. [CrossRef]

55. Marnellos, G.E.; Athanasiou, C.; Makridis, S.; Kikkinides, S. Integration of Hydrogen Energy Technologies in Autonomous Power Systems. In *Hydrogen-Based Autonomous Power Systems*; Emmanuel, I.Z., Ed.; Springer: London, UK, 2008; ISBN 978-1-84800-246-3.

56. Lisbona, P.; Corradetti, A.; Bove, R.; Lunghi, P. Analysis of a solid oxide fuel cell system for combined heat and power applications under non-nominal conditions. *Electrochim. Acta* **2007**, *53*, 1920–1930. [CrossRef]

57. Bolhàr-Nordenkampf, M.; Hofbauer, H. Biomass Gasification Combined Cycle Thermodynamic Optimisation Using Integrated Drying. In Proceedings of the ASME Turbo Expo 2004: Power for Land, Sea, and Air, Vienna, Austria, 14–17 June 2004.

58. Athanasiou, C.; Stamatelatou, A. Biogas. In *Biofuels—Sustainable Energy*; Karnavos, N., Lappas, A., Marnellos, G., Eds.; Tziolas Publishing: Thessaloniki, Greece, 2014; pp. 273–301. ISBN 978-960-418-445-3.

59. Available online: http://www.matche.com/equipcost/Blower.html (accessed on 11 July 2022).

60. Available online: www.matche.com/equipcost/Exchanger.html (accessed on 11 July 2022).

61. Whiston, M.; Azevedo, I.; Litster, S.; Samaras, C.; Whitefoot, K.; Whitacre, J. Meeting U.S. Solid Oxide Fuel Cell Targets. *Joule* **2019**, *3*, 2053–2065. [CrossRef]

62. Available online: https://www.worldcat.org/title/waste-water-treatment-technologies-a-general-review/oclc/55489914 (accessed on 26 August 2022).

63. Morandin, M.; Maréchal, F.; Giacomini, S. Synthesis and thermo-economic design optimization of wood-gasifier-SOFC systems for small scale applications. *Biomass Bioenergy* **2013**, *49*, 299–314. [CrossRef]

64. Bartoli, A.; Cavicchioli, D.; Kremmydas, D.; Rozakis, S.; Olper, A. The impact of different energy policy options on feedstock price and land demand for maize silage: The case of biogas in Lombardy. *Energy Policy* **2016**, *96*, 351–363. [CrossRef]

65. Giarola, S.; Forte, O.; Lanzini, A.; Gandiglio, M.; Santarelli, M.; Hawkes, A. Techno-economic assessment of biogas-fed solid oxide fuel cell combined heat and power system at industrial scale. *Appl. Energy* **2018**, *211*, 689–704. [CrossRef]

66. Cengel, Y.; Boles, M. *Thermodynamics: An Engineering Approach*, 8th ed.; Mc Graw-Hill Education: New York, NY, USA, 2015; ISBN 978-0-07-339817-4.